Reprogrammed SimCells for Antimicrobial Therapy

Yun Dong[1], Xianglin Ji[2], Tao Dong[3], Yun Wang[2], Erik Bakkeren[4], Kevin R. Foster[4] and Wei E. Huang[1*].

1. Department of Engineering Science, University of Oxford, Parks Road, OX1 3PJ, Oxford, UK.
2. Oxford Suzhou Centre for Advanced Research (OSCAR), University of Oxford, Suzhou Industrial Park, Jiangsu, P.R. China.
3. Department of Immunology and Microbiology, School of Life Sciences, Southern University of Science and Technology, Shenzhen 518055, China.
4. Sir William Dunn School of Pathology, University of Oxford, Oxford OX1 3RE, UK

*Corresponding author
Wei E. Huang
Tel.: +44 1865 283786
Email: wei.huang@eng.ox.ac.uk

Classification: Biological Sciences, Microbiology

Keywords: synthetic biology, SimCells, mini-SimCells, nanobody-antigen interaction, antimicrobial therapy, type VI secretion system, aspirin, catechol, hydrogen peroxide, antimicrobial resistance

Abstract

Antimicrobial resistance (AMR) is a critical global health challenge. In this study, we developed a novel platform based on chromosome-free and non-replicating simple cells (SimCells, size 1-2 µm) and mini-SimCells (size 100-400 nm) for targeted pathogen elimination. Engineered with surface-displayed nanobodies, SimCells and mini-SimCells selectively bind bacteria expressing specific antigens (e.g., OmpA in *E. coli*). The selective interactions facilitate close SimCell-pathogen proximity, enabling two antimicrobial mechanisms: direct injection of toxic effectors into bacterial cytoplasm via a heterologous expression of type VI secretion system (T6SS), and enzymatic conversion of aspirin into catechol by engineered salicylate hydroxylase, leading to sustained local production of hydrogen peroxide (H_2O_2). Our results demonstrate that both reprogrammed SimCells and mini-SimCells can eliminate target *E. coli* with high specificity and efficiency. Multi-dose reprogrammed mini-SimCell treatment led to a 10^3-fold selective reduction of targeted bacteria in mixed microbial communities, with minimal disruption to non-target bacteria. We demonstrate that reprogrammed mini-SimCells, engineered with nanobody targeting outer membrane protein OmpA of the clinically relevant multidrug resistant pathogen *E. coli* ST131, achieved elimination efficiencies over 97% at 24 and 48 hrs. This modularised 'plug-and-play' antimicrobial platform provides a highly specific, efficient and adaptable solution for combating diverse AMR pathogens.

41 **Significance Statement**

42 Antimicrobial-resistant (AMR) bacteria cause millions of deaths worldwide annually, representing a
43 critical global health challenge. In this study, we developed a novel therapeutic platform using two
44 types of chromosome-free, non-replicating engineered bacterial cells: SimCells (1–2 μm) and mini-
45 SimCells (100–400 nm). These SimCells were engineered to selectively bind to targeted *E. coli*,
46 facilitating precise delivery of toxic proteins via a Type VI secretion system (T6SS) and localised
47 generation of hydrogen peroxide from aspirin. We demonstrate that mini-SimCells eliminated over 97%
48 of a targeted AMR strain within 48 hours. Moreover, multiple-dose administration achieved a selective
49 10^3-fold reduction of targeted *E. coli* in mixed microbial communities. This modular 'plug-and-play'
50 platform offers an adaptable solution against diverse multi-drug-resistant pathogens.

51

52 **Introduction**

53 Antimicrobial resistance (AMR) is one of the top global public health challenges facing humanity by
54 the World Health Organization (WHO)(1, 2). Predicted to become the next worldwide pandemic,
55 AMR could cause over 10 million deaths annually and 100 trillion dollars of global GDP loss
56 cumulatively by 2050(3–6). Despite this urgency, the discovery of new antibiotics has stagnated. The
57 last new class of antibiotics was discovered in the 1980s(7, 8), with only recent reports in 2024
58 announcing a promising new antibiotic, zosurabalpin(9). Significant advancements in chemical
59 synthesis(10, 11), high-throughput screening(12–14), rational design(15–17), and particularly artificial
60 intelligence (AI)(18–23), have provided new pipeline for new antibiotic discovery. However, the
61 antibiotic discovery might be insufficient compared to the rapid pace and spread of AMR. It is alarming
62 that AMR has been developed for every approved antibiotic class currently being launched(24). The
63 development of alternative antimicrobial strategies has been promoted, including therapies based on
64 bacteriophage(25–27), monoclonal antibodies(28–30) and antibacterial peptides(31–33). However,
65 these approaches face limitations such as stability issues, potential toxicity, and high manufacturing
66 costs(33–35) (Supplementary Table S1).

67 Advancements in synthetic biology have led to the design of genetically engineered live
68 microorganisms for the treatment or prevention of AMR pathogens in humans(36). Various microbial
69 genetic components and tools have promoted the development of live biotherapeutic products (LBPs),
70 providing a promising approach to address metabolic disorders, cancer therapy, and other unmet
71 clinical needs(37, 38). However, biocontainment and biosafety concerns still restrain bacterial
72 therapeutics from reaching a high public acceptability(39). To mitigate safety concerns, probiotic
73 strains such as *Lactococcus lactis*(40) and *Escherichia coli* Nissle 1917 (EcN)(41, 42) have been used
74 as chassis for therapy. Alternatively, attenuated strains with native tropism or colonising features, such
75 as *Listeria*(43) and *Salmonella*(44, 45), are also employed. Despite the selection of the safety profile
76 of the chassis, the risk of uncontrolled replication remains a challenge. A few strategies, such as
77 conditional kill switches(46) and auxotrophy(47), have been used to prevent engineered bacteria from
78 proliferating uncontrollably within or outside the human body and from escaping into the environment.
79 Although these measurements restrict growth, concerns persist about the evolutionary stability of the
80 introduced genetic modification and the potential risk of horizontal gene transfer (HGT).

81 To address these challenges associated with bacterial AMR, we developed customisable platforms
82 based on SimCells (simple cell)(48) and mini-SimCells(49, 50) for use in antimicrobial therapy.
83 SimCells and mini-SimCells are chromosome-free, non-replicating and reprogrammable bacterial

84 chassis that function as "smart" bioparticles. SimCells (size 1-2 μm) are produced by removing native
85 chromosomes using tightly controlled specific endonuclease and nuclease(51, 52). Mini-SimCells
86 (size 100-400 nm) are generated through asymmetric division of bacteria with a *minD* gene
87 deletion(53–55). Both SimCells and mini-SimCells can be produced from various bacteria strains(52,
88 56) and engineered to carry designed DNA for predefined functions(49, 50) In this study, *E. coli* BL21
89 (DE3) and its ΔminD mutant were used as the chassis to generate SimCells and mini-SimCells,
90 respectively. Both SimCells and mini-SimCells cannot replicate but retain the machinery of cells (e.g.
91 transcription and translation). They are highly controllable and easy to produce from engineered
92 parental bacterial cells(49, 50) In this study, the escape frequency of SimCells is below 10^{-8}, meeting
93 the criteria of the NIH guidelines for clinical recombinant microorganisms(53). Mini-SimCells are
94 essentially engineered minicells containing designed DNA. Clinical therapy based on minicells has
95 been validated in both dogs and humans (phase I clinical trial), showing significant promise in safety
96 and efficacy(54). Remarkably, minicell-based therapy has recently been granted "Fast-Track" status
97 by the FDA(58). Hence, SimCell and mini-SimCell platforms not only meet safety standards but also
98 show great potential in clinical applications, such as pathogen and cancer treatment(49, 54, 59, 60).

99 Our strategy for antimicrobial therapy is engineering SimCells and mini-SimCells as smart 'bio-
100 particles' to selectively eradicate pathogens, while sparing non-target bacteria (Figure 1). We
101 engineered surface-displayed nanobodies on the outer membrane of SimCells and mini-SimCells using
102 a modular surface display system(61), enabling selective recognition and binding to antigens on target
103 pathogens. This nanobody-antigen interaction not only increases specificity, but also enhances
104 antimicrobial effects that rely on close cell-cell proximity (Figure 1). Such mechanisms include 'nano-
105 needle' killing via type VI secretion system (T6SS)(62, 63) and localised release of high dose of
106 antimicrobial compounds. Specifically, SimCells and mini-SimCells engineered with a modularised
107 T6SS are supposed to deliver toxic effectors(64) to the cytoplasm of other bacteria in a contact-
108 dependent manner(65–67). Another mechanism is to locally generate a high concentration of H_2O_2 via
109 catalysis of aspirin by NahG salicylate hydroxylase enzyme(68–72).

110 In this study, we engineered a customisable SimCell and mini-SimCell platform that combined both
111 mechanisms to deliver both rapid and sustained antimicrobial activity. Antimicrobial efficacy is
112 significantly enhanced by the specific binding of SimCells and mini-SimCells to target bacteria via
113 nanobody-antigen interactions, enabling immediate T6SS-mediated cytotoxicity followed by
114 prolonged hydrogen-peroxide release. For proof of concept, a single safe dose of mini-SimCells killed
115 94% of the target bacteria within 24 hours, and 99% after 48 hours. In mixed microbial communities,

four sequential doses achieved a 10^3-fold reduction of the target bacteria while leaving non-target species largely unaffected. Engineered with native-antigen targeting nanobody, reprogrammed dual mechanism mini-SimCells successfully eliminated 97% of the target multi-drug resistant pathogen, *E. coli* ST131, within 24 hrs. These findings highlight the potential of SimCells and mini-SimCells for antimicrobial therapy and set a foundation for the development of clinically safe, custom-designable biotherapeutics to combat the escalating threat of antimicrobial resistance.

Results

Surface-displayed Nanobody in E. coli Enables Selective Binding

First, the nanobodies and T6SS were characterised with the parental chassis strains before moving on to preparing SimCells and mini-SimCells. *E. coli* BL21(DE3) and its ΔminD mutant were used as the chassis to produce both SimCells and mini-SimCells. The smooth surface without flagella and fimbriae of the B lineage of *E coli* BL21(DE3) minimises interference with the nanobody-antigen interactions. It has been previously reported that an N-terminus-fusion modular system can display nanobodies on the cell's outer membrane with precise folding and efficient localisation(61). As a proof of concept, we employed a well-characterised antigen-nanobody pair, EPEA (Ag) and anti-EPEA (Nb)(73), to demonstrate the target-specific antimicrobial effect of SimCell therapy (Figure 1).

Surface-displayed nanobody expression and its antigen binding were verified at both macroscopic and microscopic levels. Strains expressing either antigen (Ag) or nanobody (Nb), as well as a null strain, were induced overnight with 100 ng/mL anhydrotetracycline (ATc), and labelled with superfolder GFP (sfGFP) (green) and mRFP (red), respectively. Stationary-phase cultures were normalised to the same optical density (OD_{600}), then left unmixed or mixed in a 1:1 ratio (Ag+Nb and Ag+Null, with the latter as a control without adhesion construct). After 12 hrs standing still, significant cell-cell aggregation was observed in cultures with adhesion pairs, while no such phenomena were seen in unmixed or control groups (Figure 2a). From these, 10 μL cultures were collected from the bottom of both adhesion and non-adhesion groups, and performed the same dilution until single cells were loosely distributed in most views under the fluorescent microscope. Cells with adhesion pairs formed mesh-like-pattern aggregates (Figure 2a). The aggregation was then quantified by measuring the OD_{600} from the upper 25% portion of the cultures (Supplementary Figure S1a). A significant OD_{600} reduction (>85%) occurred for the adhesion group (Ag+Nb) (Figure 2b). In the time-course experiment, supernatant

146 density was measured every 30 min for 3.5 hrs. The OD_{600} reduced by more than 50% for the adhesion
147 group within 1 hr (Figure 2c), indicating that Ag-Nb binding interaction is a rapid process.

148 The results suggest that the anti-EPEA Nb should be correctly folded and surface-displayed on the
149 parental chassis strains. To further test nanobody stability, Nb-expressing strains were stored at either
150 room temperature (RT), 20 °C or 4°C for 1, 5, and 10 days, then mixed with Ag-expressing *E. coli*,
151 and macroscopic aggregation was monitored for 3 hrs (Supplementary Figure S1a). There were no
152 significant cell pellets observed in all the unmixed groups, indicating cell integrity and stability.
153 Despite the extended time required to attain comparable aggregation intensity, nanobody activity was
154 preserved in cells stored at both temperatures after 10 days (Supplementary Figure S1b).

155 ***Nanobody–Antigen Pairs Enable Selective T6SS Killing of Target Cells***

156 A plasmid containing complete gene cluster encoding T6SS from *Aeromonas dhakensis*(64), has been
157 introduced to parental chassis strains (Supplementary Table S2). The plasmid contains a sfGFP-fused
158 T6SS gene cluster controlled by either a native constitutive promoter (pT6S_NP) or a tetracycline-
159 inducible promoter (pT6S_Tet), as well as inactive controls (pT6S_N3-NP and pT6S_N3-Tet), which
160 contain a noncontractile 3-amino-acid insertion in the subunits forming contractile outer sheath.
161 Fluorescence microscopy analysis demonstrated the formation of contractile tubular structures,
162 confirming T6SS activity (Figure 3a). *E. coli* BL21(DE3) engineered with T6SS also proved
163 significant killing effect in contact-promoted (solid) condition (Figure S2), confirming T6SS activity.
164 Over 97% of constitutive T6SS-expressing cells exhibited active sfGFP after 96-hour (Figure S2b) and
165 maintained significant out-competitive capability against the prey cells (Figure S2c). These results
166 indicate stable and robust expression of the T6SS across the cell population.

167 As the function of T6SS requires close cell-cell proximity and sustained interactions(74), we
168 hypothesised that nanobody-mediated selective binding could promote $T6SS^+$ attacker cells to
169 efficiently kill the targeted prey cells in a mixed population. Supplementary Figure S3a show that Nb-
170 Ag interaction enhanced T6SS-mediated killing in solid conditions. In comparison to the contact-
171 promoting killing on the solid surface, well-mixed suspension conditions are representative of clinical
172 scenarios with planktonic pathogens. The results demonstrate that in a fluid environment, the attacker
173 cells with both nanobody and active T6SS have a significant killing effect, with more than 84% of
174 prey cells eliminated compared to the negative control group. However, the attacker cells with active
175 T6SS ($T6SS^+$) without nanobodies were unable to eliminate prey cells (Figure 3b). Interestingly, an
176 inhibitory effect was also observed in the Nb-binding-only group (Figure 3b), which may be attributed
177 to the disruption of carbon-source uptake, motility, and membrane integrity in prey cells due to cell-

178 cell aggregation(75). The synergistic functionality of both binding and T6SS$^+$ was markedly more
179 pronounced. In the time-course experiment, a significant inhibition effect was detected within 4 hours
180 and continued to increase over time (Figure 3c).

181 To verify that the surviving prey cells had not acquired resistance to T6SS-mediated killing, we tested
182 various multiplicities of infection (MOI). Increased killing efficiency was observed with higher MOI,
183 suggesting that the inability to eliminate 100% of the prey cells could be due to exhaustion of T6SS
184 activity rather than prey resistance (Supplementary Figure S3b). This limitation could potentially be
185 addressed by increasing the attacker-to-prey ratio, regeneration of T6SS activity or administering
186 multiple doses.

187 To evaluate whether the nanobody display confers target specificity to T6SS$^+$ attacker cells, we co-
188 cultured the attacker cells with a mixed prey population of Ag-positive *E. coli* BL21 (Ag$^+$) and Ag-
189 negative *E coli* DH10B (Ag$^-$). Selective killing should occur only when (i) the nanobody matched the
190 paired antigen and (ii) attacker cells possessed an active T6SS. After 6 hours of co-incubation, more
191 than 50% of Ag$^+$ cells were eliminated, whereas the Ag$^-$ population showed no significant loss (Figure
192 3d and Supplementary S3c). The results confirm that nanobody-antigen interactions enabled precise
193 and T6SS-dependent elimination of the targeted prey bacteria, while sparing non-target bacteria in a
194 mixed microbial community.

195 ***T6SS Mediated Bacterial Killing in Reprogrammed SimCells***

196 Building on the demonstrated nanobody-antigen specificity and T6SS-mediated killing, we next
197 generated SimCells from our chassis strains. We previously reported the development and
198 characterisation of SimCells as a safe, reprogrammable, and customisable chassis for synthetic
199 biology(52), especially beneficial for biomedical applications such as cancer therapy(49). The
200 chromosome-free SimCells were produced by DNA cleavage at a conserved 19-bp recognition
201 sequence (contained within a 26-bp fragment) in the 23S rRNA subunit using inducible expression of
202 I-CeuI endonuclease, after which the bacterial native nuclease RecBCD initiated chromosomal
203 degradation(51).

204 Plasmids containing the I-CeuI endonuclease, the surface-displayed nanobody and the T6SS
205 machinery were introduced into the *E. coli* BL21 (DE3) chassis to produce and reprogram SimCells
206 (Supplementary Table S2). After the culture reached the early log phase (OD_{600} ~ 0.4), 1 μM of crystal
207 violet was added to induce the I-CeuI expression. Growth arrest was observed within 1 hour for
208 SimCell (+) groups, resulting in a stable OD_{600} plateau maintained for over 35 hrs of continuous

culturing, while the uninduced or control groups continued normal growth until reaching the stationary phase. For further verification, 5 μL of post-35-hr cultures were plated on LB agar, and no single colony formation was detected after 48 hrs incubation for induced SimCells (Figure 4a). Additionally, as a second validation, we stained cells with SYTO 9, a DNA-binding fluorescent dye. As expected, no significant fluorescence was observed in SimCells compared to the control group (parental cells) (Supplementary Figure S4a). Single-cell Raman analysis revealed the absence of the Raman band at 785 cm^{-1} in SimCells (Supplementary Figure S4b). Both above evidence confirm the removal of genome DNA. Finally, plating 200 μL of SimCell culture at OD_{600} = 2.0 (~10^8 cells) yielded no single colony formation after 24 hours of incubation (Supplementary Figure S4c). It confirms that the resulting SimCells had high purity, with an escape frequency of less than 10^{-8}, meeting the criteria of NIH guidelines for recombinant microorganisms(57).

We then assessed the binding ability and T6SS activity of the reprogrammed SimCells. The expression of both the nanobody and T6SS was induced prior to SimCell conversion to ensure the engineered proteins were fully assembled for operation. As shown in Figure S1c, significant macroscopic aggregation and OD_{600} reduction (>60%) were detected for the adhesion group (Ag+Nb-SimCell) after 3 hrs standing. Under the microscope, dotted GFP signals were identified as a characteristic mark for T6SS activity in most SimCells (Figure 4b). SimCells with constitutive and tetracycline-induced T6SS were generated from the cultures with the same cell density. A higher yield of functional SimCells was usually obtained for the constitutive T6SS group. The constitutive T6SS plasmid (pT6S_NP/pT6S_N3-NP) allowed the parental cells to synthesise and assemble an active secretion system before chromosome removal, reducing metabolic burden and yielding more functional T6SS SimCells than an inducible plasmid (pT6S_Tet/pT6S_N3-Tet). Hence, SimCells carrying the constitutive T6SS plasmid were used in subsequent experiments. On agar media, the T6SS activity showed significant killing effect on prey cells within 3 hrs (Supplementary Figure S4d). Nonetheless, SimCell killing efficiency was lower than that of the parental bacteria, likely due to their limited residual energy reserves.

To validate nanobody-mediated, T6SS-dependent killing by SimCells, we co-cultured antigen-positive (Ag^+) prey with attacker SimCells carrying different combinations of nanobody (Nb^+ or Nb^-) and T6SS ($T6SS^+$ or $T6SS^-$). After 6 h in minimal medium, Nb^+T6SS^+ SimCells eliminated more than 85 % of Ag^+ cells. In contrast, prey survival was roughly 50 % with nanobody binding alone (Nb^+T6SS^-), and moderate inhibition was observed with non-binding $T6SS^+$ SimCells (Nb^-T6SS^+) (Figure 4c). These

240 results confirm that SimCells retain measurable T6SS activity in suspension and demonstrate that
241 specific nanobody binding is critical for maximising T6SS-mediated killing in liquid culture.

242 ***T6SS Mediated Killing in Reprogrammed Mini-SimCells***

243 Following validation of the nanobody-directed specific T6SS killing in SimCells, we subsequently
244 established design feasibility in the mini-SimCell platform. Reprogrammed mini-SimCells were
245 generated from the aberrant cell division of the ΔminD mutant of engineered parental cells. The *E. coli*
246 BL21(DE3) ΔminD strain was previously developed and verified in our lab(49). Mini-SimCells were
247 purified by gradient centrifugation to separate them from parental cells. The formation of $T6SS^+$ mini-
248 SimCells was confirmed using fluorescence microscope (Figure 5a) and scanning electron microscope
249 (SEM) (Figure 5b). In addition, ZetaView analysis was used to characterise the size distribution of the
250 mini-SimCells, where mini-SimCells with T6SS (T6SS mini-SimCells) were identified by sfGFP-
251 labelling. Approximately 91% of mini-SimCells derived from parental cells (BL21 mini-SimCells) fell
252 within the 100-300 nm size range, while over 33% of the Nb- and T6SS-expressing mini-SimCells
253 (T6SS mini-SimCells) were larger than 300 nm (Figure 5b). This finding was consistent with the SEM
254 results, suggesting T6SS mini-SimCells were measured larger, likely due to the surface display of Nb
255 and the assembly of the T6SS machinery, as the tail length of the T6SS 'nano-needle' is dictated by
256 the size of the bacterial cell(76). ZetaView concentration analysis of the mini-SimCells revealed
257 approximately 2.20×10^{10} T6SS mini-SimCells within a total population of 3.56×10^{11} reprogrammed
258 mini-SimCells purified from the original 100 mL culture (Figure 5b). This represents a high production
259 yield, indicating promising potential for future large-scale manufacturing applications.

260 T6SS activity in mini-SimCells was verified on solid media (Supplementary Figure S5a), and
261 nanobodies enabled the T6SS to efficiently kill prey cells also in liquid media. We tested the limit of
262 killing (LOK) for Nb-T6SS mini-SimCells using a dose of 1×10^{10} Nb-T6SS mini-SimCells, which
263 has been approved as safe in previous human trials(77). Experiments were conducted at MOI of 62.5,
264 100, 500, 2500, 5000, and 10,000. As shown in Supplementary Figure S5b, significant inhibition was
265 observed across all groups, with a marked increase in killing efficiency at higher MOI. By fitting an
266 inhibitory concentration curve, the half-maximal inhibitory concentration (IC_{50}) of MOI of Nb-T6SS
267 mini-SimCells was determined to be approximately 518.5 (Figure 5c). The results demonstrate the
268 efficient prey-killing capability of our reprogrammed therapeutic mini-SimCells.

269 ***Localised H_2O_2 Generation from Parental Cells and (Mini-) SimCells***

270 In addition to the T6SS system, close contact between attacker and prey cells also allows local delivery
271 of high concentrations of antimicrobial compounds around the targeted cells. To exploit this, we

272 introduced a constitutively expressed salicylate hydroxylase (NahG) into our system (Figure S7a),
273 which catalyses the conversion of acetylsalicylic acid (aspirin) into catechol(71, 72) (Figure 6a).
274 Catechol has a broad-spectrum antimicrobial activity(68–70) by generating hydrogen peroxide (H_2O_2)
275 through autooxidation processes (Supplementary Figure S6a,b,c), during which catechol polymerises
276 to form cross-linked polymers without external catalysts(78–81) (Figure 6a). When 800 μM aspirin (a
277 non-toxic dose for humans(82)) was added to the parental cell and SimCell cultures, the filtered
278 supernatants from overnight NahG+ cultures exhibited a dark-brown colour (Supplementary Figure
279 S7b), which is associated with the oxidation products of catechol. The collected supernatants showed
280 a significant inhibitory effect on bacterial cell growth (Supplementary Figure S7b and S7c). These
281 results indicate the generation, permeability and extracellular antimicrobial activity of SimCell-
282 produced catechol and associated production of H_2O_2.

283 We then investigated co-expression of nanobody and NahG (Nb+NahG) in parental cells, SimCells
284 and mini-SimCells to eliminate targeted prey cells. The Nb+NahG parental cells, SimCells and mini-
285 SimCells were added to the prey cells at MOI of 10, 100 and 1000, along with 800 μM aspirin. As
286 shown in Figure 6b, significant inhibition was apparent in 6 hrs and pronounced across all experimental
287 groups by 24 hrs. Particularly after 48 hrs, Nb+NahG mini-SimCells eliminated over 99.9% of the
288 prey cells in the presence of a single aspirin dose. These results demonstrate that the NahG
289 reprogrammed SimCells provide a rapid and durable, aspirin-dependent antimicrobial effect.

290 Notably, NADH is required for NahG catalysis(72, 83). Prior studies suggest that mini-SimCells
291 possess a higher NADH/NAD+ ratio(84, 85), likely due to the reduced electron transport chain activity
292 resulting from the deletion of the *minD* gene and subsequent alterations in the activity of inner
293 membrane enzymes(86, 87). Along with safety and a higher specific surface area (SSA) that enhances
294 catechol penetration, mini-SimCells system is believed to be a promising platform and hence selected
295 for further experiments.

296 ***Dual-mechanism Killing Effect in Mini-SimCells***

297 Building upon these results, we evaluated an integrated mini-SimCell strategy that combines
298 nanobody-mediated binding, T6SS activity and the localised release of an antimicrobial compound. To
299 divide cellular burden and optimise the functionality of two different antimicrobial mechanisms (T6SS
300 facilitated nano-needle and NahG mediated H_2O_2 local release), we employed a consortium of Nb+
301 mini-SimCells comprising two specialised subgroups: Attacker1 (mini-SimCell Nb-T6SS) and
302 Attacker2 (mini-SimCell Nb-NahG). Non-engineered mini-SimCells (mini-SimCell Null) were used
303 as negative controls. Antigen-positive prey cells were mixed and co-cultured with various

304 combinations of engineered and control mini-SimCells in the minimal medium. After 6 hrs, 800 μM
305 aspirin was added. The T6SS-mediated attack was triggered immediately upon cell-cell contact,
306 whereas H_2O_2-based killing began after catechol production from aspirin. Delaying catechol and
307 subsequent H_2O_2 production potentially prevented these toxic metabolites from inhibiting T6SS
308 activity. Prey cell viability was quantified at 6, 24, and 48 hrs without further additions of attacker cells
309 or aspirin.

310 At an overall MOI of 250:250:1 (Attacker 1:Attacker 2:prey), each engineered mini-SimCell subgroup
311 independently reduced prey viability at different time scales, confirming the efficacy of both
312 antimicrobial modes. When combined, the dual-mechanism consortium achieved the greatest effect,
313 eliminating approximately 90% of prey cells after 48 hrs, demonstrating a synergistic antimicrobial
314 effect with two mechanisms (Figure 7a). We next tested a higher dose dual-mechanism mini-SimCells
315 to treat the target bacteria. Two types of attacker mini-SimCells were mixed with targeted prey cells at
316 MOI of 500:500:1 (Attacker 1:Attacker 2:prey) with the total mini-SimCells of 1×10^{10}, the maximum
317 tolerated dose reported in human minicell trials(77). Within the first 6 hrs, the Attacker1 (mini-SimCell
318 engineered with Nb-T6SS) rapidly eliminated over 51% of the target bacteria. Addition of 800 μM
319 aspirin enabled Attacker2 (mini-SimCell engineered with Nb-NahG) to convert aspirin to catechol and
320 generate local H_2O_2 by polymerising catechol, increasing the killing efficiency to 94.4% ±0.73% at 24
321 hrs and further reaching 99.3% ±0.29% at 48 hrs (Figure 7b).

322 To further evaluate the specificity and robustness of the platform in a complex environment, we applied
323 a multi-dose mini-SimCells to selectively target Ag^+ bacteria population within a mixed microbial
324 community. In this experiment, two distinct types of prey populations: *E. coli* BL21 with or without
325 surface-displayed EPEA antigen (Ag+/Ag-) were continuously co-cultured in a well-mixed condition.
326 To mimic periodic wash-out scenario, the cultures were diluted 1/50 with fresh medium every 24 hrs,
327 allowed to recover for 8 hrs, and then challenged with 10^{12} ++ mini-SimCells (1:1 ratio of Nb-T6SS
328 mini-SimCells : Nb-nahG mini-SimCells) or an equivalent number of the control, which is non-
329 engineered - - mini-SimCells (mini-SimCell without introduced plasmid). After each dose, co-cultures
330 were incubated for an additional 16 hrs to allow mini-SimCell mediated killing to run completely. In
331 the presence of 800 μM aspirin, four sequential doses of mini-SimCells, selective elimination of the
332 Ag^+ population was observed only in the ++ mini-SimCells treatment group (Figure 7c). Progressive
333 elimination of Ag+ cells occurred following each dual-mechanism mini-SimCell administration,
334 ultimately achieving a 10^3-fold reduction relative to the initial prey cell levels (Figure 7c). This
335 selective elimination was not observed in the control groups (- - mini-SimCell group), ruling out

336 different growth rates between Ag+ and Ag- populations in the microbial community (Figure 7c).
337 Furthermore, the Ag- population remained stable throughout the treatment experiment, confirming the
338 specificity of the target elimination (Figure 7c). Collectively, these results demonstrate the potent and
339 sustained antimicrobial activity of dual-mechanism mini-SimCells. The combination of rapid T6SS-
340 mediated killing with prolonged NahG-driven H_2O_2 production has effectively and selectively
341 eradicated targeted cells in mixed communities while sparing non-target populations.

342 ***Reprogrammed Mini-SimCells Effectively Targeted and Eliminated E. coli ST131, an AMR***
343 ***Pathogenic Strain***

344 Building on the proof-of-concept platform demonstrating SimCell- and mini-SimCell-based targeted
345 antimicrobial activities in mixed communities, we then evaluate the system against a clinically relevant
346 multidrug-resistant pathogen. *E. coli* ST131 represents a globally dominant AMR strain responsible
347 for a substantial proportion of urinary tract and bloodstream infections(88–91). It raises clinical
348 concern particularly because of its resistance to fluoroquinolones and β-lactam antibiotics due to its
349 extended-spectrum β-lactamases (ESBLs)(89, 92). The WHO has classified ESBL-producing *E. coli*,
350 including ST131, as a high-to-critical priority AMR pathogen, underscoring the urgent need for novel
351 therapeutic strategies targeting this AMR strain (93). Hence *E. coli* ST131 (NCTC 13441) strain was
352 selected for the evaluation of the SimCell efficacy against AMR pathogens.

353 To achieve specific recognition of *E. coli* ST131, we engineered (mini-)SimCells to express
354 nanobodies targeting outer membrane protein (OmpA). Specifically, we used Nb39, a nanobody
355 exhibiting high binding affinity and specificity for the long OmpA isoform (OmpA-L) in *E. coli*
356 isolates(94). We engineered Nb39 fused with the N-terminal modular system for surface display in the
357 parental strain of mini-SimCells. Stationary-phase cultures of *E. coli* ST131 and Nb39-displaying cells
358 (BL21:Nb39-mRFP) were adjusted to the same OD_{600}, mixed at a 1:1 ratio, and allowed to settle
359 overnight undisturbed. *E. coli* BL21(DE3) strains engineered with surface displayed synthetic antigen
360 (BL21: Ag), EPEA, were used as the unrecognised control and mixed with Nb-39-displaying cells. *E.*
361 *coli* ST131 and BL21: Ag cells were pre-stained with SYTO 9, while Nb39-displaying cells were
362 genetically labelled with mRFP for fluorescence tracking. Figure 8a shows parental cells (expressing
363 mRFP) with Nb39 surface display bond to *E. coli* ST131 (SYTO9 staining). Significant cell-cell
364 aggregates were observed under fluorescence microscopy (Figure 8a Left), whilst the control showed
365 scattered cell distribution (Figure 8a Right). Aggregation of these cells was mediated by the
366 interactions of the OmpA-L antigen and Nb39 nanobody. Flow cytometry detected single events
367 exhibiting both green and red fluorescence (G+R), designated as "doublets". Flow cytometry analysis

368 demonstrated that 46.4% of the population exhibited doublet characteristics (Figure 8b Left), whilst
369 the control had 0.0% doublets (Figure 8b Right). It indicates the efficient targeting at *E. coli* ST131
370 via Nb39-mediated antigen recognition. These results confirm that surface-displayed Nb39 enables
371 specific and robust binding to *E. coli* ST131 through native antigen (OmpA-L) recognition, preparing
372 for the targeted mini-SimCells killing.

373 Subsequently, we demonstrate that reprogrammed mini-SimCells achieved efficient elimination of the
374 multidrug-resistant pathogenic strain *E. coli* ST131 (Figure 8c). Nb39-displaying mini-SimCells
375 equipped with either T6SS (mini-SimCell: Nb39-T6SS) or nahG (mini-SimCell: Nb39-nahG) modules
376 were evaluated for their antimicrobial efficacy. *E. coli* ST131 elimination assays were conducted at an
377 overall MOI of 500:500:1 (Attacker 1: Attacker 2: Prey), with a total mini-SimCell number of 1×10^{10}.
378 Mini-SimCells equipped with nanobody-directed T6SS achieved >70% elimination of *E. coli* ST131
379 at 6 hrs (Figure 8c). When 800 μM aspirin was supplemented, the converted catechol and locally
380 generated H_2O_2 further enhanced antimicrobial activity. Hence, the dual-mechanism mini-SimCell
381 consortium increased the elimination efficiency to 97.19% ±0.97% at 24 hrs and 97.58% ±1.05% at
382 48 hrs (Figure 8c). In contrast, *E. coli* ST131 exhibited persistent resistance to broad-spectrum β-
383 lactam antibiotics, with no growth inhibition observed for benzylpenicillin (PenG) and cefotaxime
384 even at 100 μg/mL (supplementary Figure S8a and S8b). These results demonstrate that the nanobody-
385 targeted, dual-mechanism mini-SimCell platform can overcome conventional antibiotic resistance
386 mechanisms to achieve potent, specific elimination of clinically relevant multidrug-resistant pathogens.

387

388 **Discussion**

389 In this study, we introduce a novel SimCell and mini-SimCell platform with antimicrobial properties.
390 Through nanobody-antigen binding, the reprogrammed SimCells and mini-SimCells are designed to
391 selectively eliminate target cells via T6SS-mediated killing within 4-6 hrs and local conversion of
392 aspirin to catechol, which then continuously generates high-concentration of H_2O_2 over several days.
393 This antimicrobial strategy provides both immediate and sustained antimicrobial effects, offering the
394 potential for controlling acute bacterial infection and preventing reoccurrence. For proof-of-concept,
395 our results demonstrate that the mini-SimCell consortium can eliminate 94.4% of target prey cells in
396 24 hrs, and 99.3% in 48 hrs with a single dose of mini-SimCells at MOI of 1000:1. Our results also
397 demonstrate the selective pathogen depletion up to 10^3-fold within the mixed microbial communities
398 using multi-dose mini-SimCell administration. This observation further validates the specific
399 antimicrobial efficacy of the platform. To demonstrate the anti-AMR capacity and clinical application
400 potential of our reprogrammed (mini-)SimCell-based therapeutic platform, we adapted the system to
401 target the clinically relevant, multidrug-resistant pathogenic strain *E. coli* ST131. Equipped with a
402 native OmpA recognising nanobody (Nb39), our reprogrammed mini-SimCells achieved 97.19%
403 target pathogen elimination within 24 hours, overcoming conventional antibiotic resistance
404 mechanisms. This success against a high-to-critical priority AMR pathogen demonstrates the
405 translational potential of our platform for addressing urgent clinical challenges posed by multidrug-
406 resistant infections. The combination of antibacterial efficacy and selectivity represents a significant
407 advancement over broad-spectrum antimicrobial approaches, positioning this platform as a promising
408 next-generation therapeutic strategy for combating antimicrobial resistance.

409 We vision this platform as a new approach for developing clinically safe, custom-designable
410 biotherapeutic products against multi-drug-resistant pathogens. The key attributes and advantages of
411 this platform include the following aspects: 1) Biosafety. SimCells and mini-SimCells met the criteria
412 of NIH-recommended escape frequency threshold - one live cell from 10^8 SimCells (57). Minicells
413 derived from *Salmonella typhimurium,* which are similar to *E. coli* derived mini-Simcells, have been
414 granted US FDA approval for human trial (https://engeneic.com/), and proven safe without adverse
415 effect in human phase I clinical trial (95). To further enhance biosafety, our platform will be extended
416 to use SimCells and mini-SimCells derived from LPS-free *E. coli* BL21(DE3) chassis (ClearColi)(96).
417 2) Antimicrobial specificity and efficacy. SimCell and mini-SimCell chassis are highly controllable
418 while maintaining robust bioactivity against target bacteria. The precise targeting helps to minimise
419 unintended effects on non-targeted microbes, enhancing the therapeutic efficacy. 3) Modularity and

420 customisability. This modular platform features a versatile architecture that allows for easy redesign
421 in a “plug-and-play” manner. Surface-displayed nanobodies can be systematically reconfigured to
422 target a specific new pathogen, enhancing the adaptability of the platform. Additionally, T6SS
423 effectors can be engineered and seamlessly integrated into the existing modules. The enzyme-catalysis
424 mechanism for converting pro-drugs to antimicrobial compounds, such as the aspirin-catechol system,
425 can also be redesigned to fit specific therapeutic needs. 4) Scalability. SimCells and mini-SimCells
426 can be easily produced and purified from engineered parent cells, making them suitable for large-scale
427 industrial manufacturing. The streamlined production process, combined with high yield and cost-
428 effective scalability, offers a manufacturing practical solution to address the urgent challenges posed
429 by AMR.

430 The historic battle between humans and bacterial pathogens has intensified since the “Golden Age” of
431 antibiotic discovery in the 1950s(8). Today, only a limited number of small molecules are currently
432 undergoing clinical trials as potential antibiotic candidates, with nearly half being new beta-lactamase
433 inhibitors used with established beta-lactam antibiotics(97). Recent advances in AI and machine
434 learning (ML) have accelerated antibiotic discovery and design. A landmark study employed a deep
435 neural network to identify a novel broad-spectrum antibiotic, halicin(22), followed by works utilising
436 machine learning models to discover new antibiotics against drug-resistant *Acinetobacter*
437 *baumannii*(19, 20). A recent work for the first time *de novo* designed structurally novel antibiotics for
438 drug-resistant gonorrhoea and MRSA via a generative deep learning approach(23). Despite these
439 advances, the "black box" nature of some AI models can obscure the rationale behind predictions and
440 limit the exploration of chemical spaces. Hence, researchers are now actively working on interpretable
441 AI models(21). Additionally, validation of these in silico predictions and data collection for model
442 training still requires extensive experimental tests.

443 Traditional chemical-based antibiotics face an evolutionary paradox: while effectively eliminating
444 susceptible bacteria, they also promote the survival and spread of resistant variants, inadvertently
445 advancing AMR with each treated infection(98). In response, alternative antimicrobials have been
446 developed, including antimicrobial peptides, bacteriophage, and monoclonal antibodies. Each
447 approach faces its challenges, such as biosafety, stability and the potential risk of rapid resistance
448 development (Supplementary Table S1). Several studies have reported the antimicrobial effects of
449 bacteria engineered to neutralise virulence(99, 100) or eradicate pathogens. To selectively inhibit the
450 target bacteria, toxic cargos were delivered by conditional lysis-based release(101, 102) or cytoplasm-
451 translocation via conjugation(103–105). Nonetheless, balancing high efficacy with the management of

452 side effects (e.g. endotoxin release during lysis) remains a challenge for these approaches. In contrast,
453 the highly controllable and safe SimCells and mini-SimCells are reprogrammed to selectively target
454 pathogens through surface-displayed nanobodies and efficiently eliminate the target cells, using
455 contact-dependent antimicrobial strategies.

456 This study established a modular antimicrobial platform as proof of concept, and further successfully
457 demonstrates its adaptability using a native-antigen-targeting nanobody against a multi-drug resistant
458 pathogen from a clinical isolate. In real world clinical practice, the surface antigens of AMR pathogens
459 could change due to mutations and environmental factors, potentially affecting epitope accessibility.
460 The modularised design of mini-SimCell platform can be rapidly adapted to equip new nanobodies in
461 response to the changes of surface antigens in AMR pathogens. We expect to further expand nanobody
462 reservoirs targeting antigens from various multi-drug-resistant pathogens and resembling diverse
463 clinical scenarios. The current landscape of nanobody discovery relies on immunity-based
464 approaches(106), which restricts diversity and availability. Emerging strategies, such as the
465 combination of bioinformatics-driven antigen mining and high-throughput library(107, 108), AI
466 enabled *de novo* protein design(109, 110) and deep learning models(111), offer promising approaches
467 to overcome the limitations and accelerate the expansion of the nanobody repertoire for next generation
468 of precise antimicrobials. The dual-mechanism platform in this study broadly targets evolutionarily
469 conserved cellular processes, via T6SS 'nano-needle' spearing and H_2O_2 toxicity, minimising the
470 likelihood of resistance development. However, antigen mutations could possibly enable the prey cell
471 to escape from being recognised and targeted. Hence, the development of multiple nanobodies that
472 target different antigens of AMR pathogens could be a potential solution.

473 T6SS represents a worth-noting strategy in this study. Building on previous research that uses native
474 T6SS as controllable weapons against target pathogens(112, 113), our work advances the field by
475 heterologously expressing and assembling functional T6SS in SimCell and mini-SimCell chassis,
476 enhancing T6SS-based biotherapeutic applications. The natural diversity of T6SS's effectors and
477 targets provides a foundation for expanding the functionality of engineered T6SS in this SimCell
478 platform to antimicrobial-resistant Gram-positive bacteria and fungi(114). Engineered T6SS could
479 also deliver various protein payloads, such as Cas9(115) and Cre recombinase(116), directly to the
480 cytoplasm of target pathogens. SimCell and mini-SimCell chassis also minimise environment
481 disruption *in situ*, with the versatility of T6SS opening possibilities for a wide range of biotherapeutic
482 interventions(115) and ecological modification of microbial communities(117).

483 In conclusion, the reprogrammed antimicrobial SimCell and mini-SimCell platform described in this
484 study offers a novel approach for tackling global bacterial AMR challenges. This work exemplifies
485 the potential of synthetic biology to revolutionise biotherapeutic applications, demonstrating an
486 innovative and effective approach to combat persistent and emerging AMR threats.

487

488 **Materials and Methods**

489 **Bacterial strains and growth conditions**

490 All strains used in this study are listed in Supplementary Table S2. *E. coli* DH5α and DH10B were
491 used for cloning and plasmid maintenance. *E. coli* BL21(DE3) was used for the function test and
492 SimCell generation. E. *coli* BL21(DE3) ΔminD was used for mini-SimCell generation. Heat shock and
493 electroporation methods were used for chemical transformation for both strains. Above cells were
494 cultured in Luria−Bertani (LB) media or M9 minimal media with specific nutrient supplements (0.4%
495 glucose, 0.2% casamino acids, 1x trace elements) at 37 °C, 180 rpm. *E. coli* ST131 (NCTC 13441)
496 cells were cultures in M9 minimal media with 0.4% glucose and 1mM EDTA at 37 °C, 180 rpm.
497 Corresponding antibiotics were used for selection: 25 μg/mL chloramphenicol, 50 μg/mL kanamycin,
498 50 μg/mL carbenicillin, 100 μg/mL streptomycin or 25 μg/mL cefotaxime. Corresponding inducers
499 were used for induction: 100 ng/mL anhydrotetracycline (ATc), 0.2% arabinose (Ara) or 1 μM crystal
500 violet. Strain stocks were stored in 20% glycerol at -80 °C for long-term storage. Agar plates were
501 kept at 4 °C for short-term storage.

502 **Plasmid construction**

503 All plasmids used in this study are listed in Supplementary Table S2. Plasmids were obtained from lab
504 storage, purchased from Addgene (pDSG287, pDSG289, pDSG291) or as gifts from collaborators. Q5
505 high-fidelity DNA polymerase (New England Biolabs) was used for DNA fragment amplification.
506 NEBuilder HiFi DNA Assembly (New England Biolabs) was used for plasmid construction.
507 DreamTaq Green PCR Master Mix (Thermo Fisher Scientific) was used for colony PCR. DNA stocks
508 were stored at -20 °C.

509 **Macroscopic and microscopic aggregation assays**

510 Cultures were grown at 37°C, 180 rpm in 50 mL LB with corresponding antibiotics in a 200 mL flask
511 for 24 hours to ensure stationary phase. All cultures were centrifuged at 3500 rpm for 20 min,
512 resuspended with 1xPBS solution, then adjusted to an initial OD_{600} of 0.8. Cultures were mixed in a
513 1:1 v:v ratio (total volume 3mL) in 5 mL clear polypropylene tubes. For macroscopic aggregation, 100

514 μL of sample was collected from the top 25% supernatant for each measurement. OD_{600} measurements
515 were read by Synergy 2 microplate reader (BioTek). For microscopic aggregation, 100 μL of the
516 sample was collected from the bottom of the overnight settled mixture and then diluted to an
517 appropriate concentration for fluorescence microscopy using Nikon Ti Eclipse. Fiji was used for image
518 analysis.

519 **Bacterial Killing Assay**

520 For parental cells, overnight cultures of attacker and prey cells were transferred into fresh LB medium
521 with corresponding antibiotics at a ratio of 1:100 and grown to an OD_{600} = 1, the inducer was added
522 when OD_{600} reached 0.6 if needed. Cells were harvested by centrifugation at 1,500 g for 10 min, and
523 the pellets were resuspended in fresh LB or M9 minimal media. For SimCells and mini-SimCells, cell
524 pellets were washed twice with fresh LB or M9 minimal media to fully remove the crystal violet or
525 antibiotics. Cell suspensions were normalised to an initial OD_{600}. Mixtures of attacker and prey cells
526 were then established at intended v:v or n:n ratios, cell number is calculated as(118, 119):

527 $$N_{\text{Parental cells / SimCells}} = A_{600} \times 8.0 \times 10^{8}/\text{mL}$$

528 $$N_{\text{mini_SimCells}} = A_{600} \times 5.0 \times 10^{10}/\text{mL}$$

529 For solid (contact-promoting) condition, triplicates of 5 μL of each mixture were spotted on LB / M9
530 agar plates (inducer was added if needed) and incubated at 37°C for 3 hours. Cells were then harvested
531 by excising individual spots from the agar plates into LB medium. For liquid (well-mixed) conditions,
532 mixtures of attacker and prey cells were established then incubated at 37°C, 180rpm for 2, 4, 6, 8, 24,
533 48 hrs. Suspensions were serially diluted and plated on selective media (selection for prey cells) for
534 quantification of CFUs, then assessed the survival of prey cells. Survival rate was calculated as:

535 $$\text{Survival rate} = \frac{\text{Survival cell}}{\text{total prey cell}} \times 100\%.$$

536 Killing efficiency was calculated as:

537 $$\text{Killing (or elimination) efficiency} = 1 - \text{survival rate}$$

538 **SimCell purification and characterisation**

539 For T6SS-assembled SimCells, overnight cultures were transferred into fresh LB medium with
540 corresponding antibiotics at a ratio of 1:100 and grown at 37 °C, 180 rpm to an OD_{600} = 1, inducer was
541 added when OD_{600} reached 0.6 if needed. For NahG-expressing SimCells, overnight cultures were
542 directly used. Cells were collected by 1500 g centrifuge for 10 min at room temperature, washed twice,
543 and resuspended with M9 + 0.2% casamino acids media, inducer was added if needed. 1μM of crystal
544 violet was added to induce SimCell conversion. Incubated overnight at 37 °C, 180 rpm. Then
545 ceftriaxone (100 μg/mL), penicillin G (100 μg/ mL), and cefotaxime (100 μg/mL) were added to the

546 culture and further incubated at 37 °C, 180 rpm for 4 hours. 100 μL of cultures were plated for purity
547 check and the rest were kept at 4 °C for further use. Cultures were washed twice with 1×PBS to remove
548 the crystal violet and antibiotics before being used for bacterial killing assay.

549 **Growth arrest assay**

550 Overnight cultures were diluted in 1:1000 ratio in 200 μL LB with corresponding antibiotics in a flat
551 96-well plate. The plate was sealed with a Breathe-Easy sealing membrane and incubated with Synergy
552 2 microplate reader (BioTek) at 37 °C, 1000 rpm. OD_{600} was measured every 15min since incubation.
553 After 2-3 hours, OD_{600} reached ~0.3, 0.2 μL of crystal violet to induce the SimCell conversion. OD_{600}
554 were continuously measured for over 35 hours.

555 **Plating assay**
556 The culture (5 μL) from each group was extracted and dot-plated in LB agar without antibiotics. Plates
557 were incubated for 24 hr at 37 °C then images were collected to record the colony growth conditions.

558 **Mini-SimCell production and purification**
559 For T6SS-assembled mini-SimCells, overnight cultures were 1:100 inoculated into 100mL fresh LB
560 medium with corresponding antibiotics and grown at 37 °C, 180 rpm to an OD_{600} = 1, inducer was
561 added when OD_{600} reached 0.6 if needed. For NahG-expressing SimCells, 100mL of overnight cultures
562 were directly used. The culture was centrifuged at 2000 g for 10 min at 4 °C to remove the normal-
563 size cells, the supernatant was retained for further centrifugation at 12,000 g for 15 min at 4 °C. The
564 pellet was resuspended in 1 mL of fresh LB and pooled together. Ceftriaxone (100 μg/mL), penicillin
565 G (100 μg/ mL), and cefotaxime (100 μg/mL) were added to the culture and incubated at 37 °C, 180
566 rpm overnight. The culture was first centrifuged at 500 g for 10 min at 4 °C to remove cell debris.
567 Then the supernatant was retained and further centrifuged at 12,000 g for 15 min at 4 °C to collect the
568 mini-SimCells. The final pellet was resuspended in 1 mL of 1xPBS solution and stored at 4 °C until
569 further use. Cultures were washed twice with 1xPBS to remove the antibiotics before being used for
570 bacterial killing assay. 5uL of each sample was used for plating assay to verify the purity.

571 **Mini-SimCell size distribution and concentration characterisation**
572 The size distribution and concentration of Mini-SimCells were characterised by nanoparticle tracking
573 analysis (NTA) using ZetaView (Particle Metrix, Inning am Ammersee, Germany). Prior to the
574 measurement, Silica 100 nm microspheres (Polysciences Inc., Philadelphia, United States) were used
575 for the quality check. Purified mini-SimCells were diluted in 1xPBS to an optimal concentration. The

576 same batch of 1xPBS solution was used as the control group. 1mL of each sample was loaded onto the
577 sample chamber using a syringe to avoid introducing bubbles. Background 1×PBS was used for
578 flushing away the previous sample before loading a new sample. In the sample chamber, mini-
579 SimCells were illuminated by a laser beam, the scattered light was captured, and the movement of each
580 particle over time was tracked by a live camera. Based on Brownian motion, the diffusion coefficient
581 of the particles was calculated, and then the size of each particle was determined using the Stokes-
582 Einstein equation. Mini-SimCell concentrations were calculated by the number of particles in a known
583 volume compared to the control group. Each sample was measured from 11 positions in 2 cycles.
584 Parameter set as: sensitivity = 80, frame = 30, shutter speed = 100. For T6SS Mini-SimCells, a 500
585 nm filter was added to observe the fluorescent particles selectively.

586 **Multi-dose dual-mechanism mini-SimCell consortium Killing Assay**

587 *E. coli* with and without surface-displayed EPEA epitope were designated as Ag+ and Ag- strains
588 respectively. Both strains were grown overnight in LB medium at 37 °C with shaking at 180 rpm, then
589 normalised to an OD_{600}=1.25. Equal volume (20 µL) of each culture was co-inoculated into 1 mL of
590 fresh LB in 1.5 mL Eppendorf tubes for 24 hrs to establish a steady status of the mixed population.
591 Following incubation, 20 µL of each co-culture was collected for serial dilution and plated on selective
592 plates for prey cells and counted colony forming units (CFUs), defining this as Day 0. Aspirin was
593 then added into LB medium with a final concentration of 800 µM. Fresh mini-SimCells were prepared
594 daily for every treatment dose. The engineered dual-mechanism ++ mini-SimCells consisted of
595 Attaker1: mini-SimCell Nb-T6SS and Attaker2: mini-SimCell Nb-NahG at an n:n ratio of 1:1. The
596 non-engineered - - mini-SimCells were served as negative control. For each dose, 100 µL 10^{12} ++ / - -
597 mini-SimCells were well-mixed and then added into the co-culture. The first dose of ++ / - - mini-
598 SimCells was added after initial 24-hr incubation, followed by an additional 16 hrs incubation at 37 °C,
599 180 rpm. Afterwards, 20 µL of the co-cultures were collected for plating and CFU counting (Day 1).
600 The co-cultures were then diluted 1:50 into fresh LB medium containing 800 µM aspirin, and
601 incubated at 37 °C, 180rpm for 8 hrs. This process was repeated for the 2nd , 3rd , 4th doses of mini-
602 SimCells (Day 2,3,4).

603 **Double-color Flow Cytometry Assay for Binding Population Quantification**

604 Overnight *E. coli* ST131 cultures was 1:100 inoculated in 5 mL M9 minimal media with 0.4% glucose
605 and 1 mM EDTA, then grew at 37°C, 180 rpm for 48 hrs. BL21:Ag and BL21: Nb39-mRFP strains
606 were 1:100 inoculated at 37°C, 180 rpm in 5 mL LB medium and grew overnight. All cultures were
607 centrifuged at 1500 g for 10 min, washed twice and resuspended with 1mL 1xPBS solution. *E. coli*

608 ST131 and BL21:Ag cultures were stained with 1uM of SYTO 9 dye at room temperature for 2 hrs in
609 dark. Then all cultures washed twice with 1xPBS solution and resuspended with 1xPBS solution,
610 OD_{600} normalised to 1.0. *E. coli* ST131/ BL21:Ag and BL21: Nb39-mRFP cultures were mixed in v:v
611 / 1:1 ratio in total volume of 1.5mL. Mixed cultures were settled still in dark overnight. Each culture
612 was 1:100 diluted with 1×PBS solution and used for FACS analysis. BD Aria Fusion was used for
613 flow cytometry analysis.

614

Data Availability Statement: The data generated in this study are provided in the main text and/or Supplementary information, where the source data are listed in the Source Data file. Source data are provided with this paper.

Acknowledgements

W.E.H. thanks EPSRC (EP/M002403/1 and EP/Y014073/1) for financial support. Y.D. gratefully acknowledges support from Oxford Interdisciplinary Bioscience DTP, funded by BBSRC (BB/T008784/1). K.R.F. is funded by Wellcome Trust Investigator award 209397/Z/17/Z and European Research Council Grant 787932**.** We thank Harris Saeed from the Engineering Department, University of Oxford, for helping with the SEM. Sample process and image for SEM were conducted at the Sir William Dunn School of Pathology, University of Oxford. We would like to acknowledge Dr. Naveed Akbar from the Radcliffe Department of Medicine, University of Oxford, for providing ZetaView equipment and technical expertise, and Vasiliki Tsioligka from the Flow Cytometry Facility, Sir William Dunn School of Pathology, University of Oxford, for providing flow cytometry technical expertise. We also thank all members of the Huang lab for the discussions and support.

Author Contributions Statement: W.E.H conceived the original idea; Y.D. and W.E.H. designed research; Y.D. and X.J. performed research; X.J. T.D. Y.W. and E.B. contributed new reagents/analytic tools. Y.D., K.R.F. and W.E.H. analysed and interpreted data; Y.D. and W.E.H. drafted the manuscript; W.E.H. and K.R.F. provided supervision; all authors reviewed and revised the manuscript.

Competing Interests Statement: Y.D. and W.E.H. have filed a provisional patent application with the UK Patent Office related to this work.

References

1. Antimicrobial resistance. Available at: https://www.who.int/health-topics/antimicrobial-resistance [Accessed 1 December 2024].
2. WHO, WHO bacterial priority pathogens list, 2024: Bacterial pathogens of public health importance to guide research, development and strategies to prevent and control antimicrobial resistance. *Bacterial pathogens of public health importance to guide research, development and strategies to prevent and control antimicrobial resistance* 72 (2024).
3. M. Naghavi, *et al.*, Global burden of bacterial antimicrobial resistance 1990–2021: a systematic analysis with forecasts to 2050. *The Lancet* **404**, 1199–1226 (2024).
4. J. O'Neill, Tackling drug-resistant infections globally: final report and recommendations. [Preprint] (2016). [Accessed 15 October 2024].
5. C. J. Murray, *et al.*, Global burden of bacterial antimicrobial resistance in 2019: a systematic analysis. *The Lancet* **399**, 629–655 (2022).
6. Global AMR R&D Hub and WHO, "Incentivising the Development of New Antibacterial Treatments 2024: Progress Report by the Global AMR R&D Hub and WHO" (2024).
7. M. Miethke, *et al.*, Towards the sustainable discovery and development of new antibiotics. *Nature Reviews Chemistry 2021 5:10* **5**, 726–749 (2021).
8. L. L. Silver, Challenges of antibacterial discovery. *Clin Microbiol Rev* **24**, 71–109 (2011).
9. C. Zampaloni, *et al.*, A novel antibiotic class targeting the lipopolysaccharide transporter. *Nature 2024 625:7995* **625**, 566–571 (2024).
10. P. M. Wright, I. B. Seiple, A. G. Myers, The Evolving Role of Chemical Synthesis in Antibacterial Drug Discovery. *Angewandte Chemie International Edition* **53**, 8840–8869 (2014).
11. B. Goel, N. Tripathi, N. Bhardwaj, I. Pal Singh, S. K. Jain, Semisynthesis: An Essential Tool for Antibiotics Drug Discovery. *ChemistrySelect* **9**, e202400554 (2024).
12. N. J. Ayon, High-Throughput Screening of Natural Product and Synthetic Molecule Libraries for Antibacterial Drug Discovery. *Metabolites 2023, Vol. 13, Page 625* **13**, 625 (2023).
13. B. Blasco, *et al.*, High-throughput screening of small-molecules libraries identified antibacterials against clinically relevant multidrug-resistant A. baumannii and K. pneumoniae. *EBioMedicine* **102**, 105073 (2024).
14. T. C. Scanlon, S. M. Dostal, K. E. Griswold, A high-throughput screen for antibiotic drug discovery. *Biotechnol Bioeng* **111**, 232–243 (2014).
15. G. König, *et al.*, Rational prioritization strategy allows the design of macrolide derivatives that overcome antibiotic resistance. *Proc Natl Acad Sci U S A* **118**, e2113632118 (2021).
16. T. F. Durand-Reville, *et al.*, Rational design of a new antibiotic class for drug-resistant infections. *Nature 2021 597:7878* **597**, 698–702 (2021).
17. R. D. Miller, *et al.*, Computational identification of a systemic antibiotic for gram-negative bacteria. *Nat Microbiol* **7**, 1661 (2022).
18. A. Talat, A. U. Khan, Artificial intelligence as a smart approach to develop antimicrobial drug molecules: A paradigm to combat drug-resistant infections. *Drug Discov Today* **28**, 103491 (2023).
19. K. Swanson, *et al.*, Generative AI for designing and validating easily synthesizable and structurally novel antibiotics. *Nature Machine Intelligence 2024 6:3* **6**, 338–353 (2024).
20. G. Liu, *et al.*, Deep learning-guided discovery of an antibiotic targeting Acinetobacter baumannii. *Nature Chemical Biology 2023 19:11* **19**, 1342–1350 (2023).
21. F. Wong, *et al.*, Discovery of a structural class of antibiotics with explainable deep learning. *Nature 2023 626:7997* **626**, 177–185 (2023).
22. J. M. Stokes, *et al.*, A Deep Learning Approach to Antibiotic Discovery. *Cell* **180**, 688-702.e13 (2020).

23. A. Krishnan, *et al.*, A generative deep learning approach to de novo antibiotic design. *Cell* **188**, 5962-5979.e22 (2025).
24. N. S. Devi, *et al.*, Overview of antimicrobial resistance and mechanisms: The relative status of the past and current. *The Microbe* **3**, 100083 (2024).
25. A. Bruttin, H. Brüssow, Human volunteers receiving Escherichia coli phage T4 orally: A safety test of phage therapy. *Antimicrob Agents Chemother* **49** (2005).
26. A. Wright, C. H. Hawkins, E. E. Änggård, D. R. Harper, A controlled clinical trial of a therapeutic bacteriophage preparation in chronic otitis due to antibiotic-resistant Pseudomonas aeruginosa; a preliminary report of efficacy. *Clinical Otolaryngology* **34**, 349–357 (2009).
27. E. Criscuolo, S. Spadini, J. Lamanna, M. Ferro, R. Burioni, Bacteriophages and Their Immunological Applications against Infectious Threats. *J Immunol Res* **2017**, 3780697 (2017).
28. A. DiGiandomenico, B. R. Sellman, Antibacterial monoclonal antibodies: the next generation? *Curr Opin Microbiol* **27**, 78–85 (2015).
29. I. Lowy, *et al.*, Treatment with Monoclonal Antibodies against Clostridium difficile Toxins . *New England Journal of Medicine* **362**, 197–205 (2010).
30. L. M. Guachalla, *et al.*, Multiple modes of action of a monoclonal antibody against multidrug-resistant Escherichia coli sequence type 131-H30. *Antimicrob Agents Chemother* **61** (2017).
31. C. D. Fjell, J. A. Hiss, R. E. W. Hancock, G. Schneider, Designing antimicrobial peptides: form follows function. *Nature Reviews Drug Discovery 2012 11:1* **11**, 37–51 (2011).
32. C. D. Santos-Júnior, *et al.*, Discovery of antimicrobial peptides in the global microbiome with machine learning. *Cell* **187**, 3761-3778.e16 (2024).
33. C. Bucataru, C. Ciobanasu, Antimicrobial peptides: Opportunities and challenges in overcoming resistance. *Microbiol Res* **286**, 127822 (2024).
34. F. Plisson, O. Ramírez-Sánchez, C. Martínez-Hernández, Machine learning-guided discovery and design of non-hemolytic peptides. *Scientific Reports 2020 10:1* **10**, 1–19 (2020).
35. F. L. Gordillo Altamirano, J. J. Barr, Phage therapy in the postantibiotic era. *Clin Microbiol Rev* **32** (2019).
36. U.S. Department of Health and Human Services Food and Drug Administration, Early Clinical Trials with Live Biotherapeutic Products: Chemistry, Manufacturing, and Control Information; Guidance for Industry. (2016).
37. D. T. Riglar, P. A. Silver, Engineering bacteria for diagnostic and therapeutic applications. *Nature Reviews Microbiology 2018 16:4* **16**, 214–225 (2018).
38. A. Cubillos-Ruiz, *et al.*, Engineering living therapeutics with synthetic biology. *Nature Reviews Drug Discovery 2021 20:12* **20**, 941–960 (2021).
39. M. Mimee, R. J. Citorik, T. K. Lu, Microbiome therapeutics — Advances and challenges. *Adv Drug Deliv Rev* **105**, 44–54 (2016).
40. T. V. Plavec, A. Berlec, Engineering of lactic acid bacteria for delivery of therapeutic proteins and peptides. *Applied Microbiology and Biotechnology 2019 103:5* **103**, 2053–2066 (2019).
41. J. P. Lynch, L. Goers, C. F. Lesser, Emerging strategies for engineering Escherichia coli Nissle 1917-based therapeutics. *Trends Pharmacol Sci* **43**, 772–786 (2022).
42. U. Sonnenborn, Escherichia coli strain Nissle 1917—from bench to bedside and back: history of a special Escherichia coli strain with probiotic properties. *FEMS Microbiol Lett* **363** (2016).
43. A. Wallecha, P. C. Maciag, S. Rivera, Y. Paterson, V. Shahabi, Construction and characterization of an attenuated Listeria monocytogenes strain for clinical use in cancer immunotherapy. *Clinical and Vaccine Immunology* **16**, 96–103 (2009).
44. R. P. Aganja, C. Sivasankar, A. Senevirathne, J. H. Lee, Salmonella as a Promising Curative Tool against Cancer. *Pharmaceutics* **14**, 2100 (2022).
45. M. Loeffler, G. Le'Negrate, M. Krajewska, J. C. Reed, Attenuated Salmonella engineered to produce human cytokine LIGHT inhibit tumor growth. *Proc Natl Acad Sci U S A* **104**, 12879–12883 (2007).

46. C. T. Y. Chan, J. W. Lee, D. E. Cameron, C. J. Bashor, J. J. Collins, "Deadman" and "Passcode" microbial kill switches for bacterial containment. *Nature Chemical Biology 2015 12:2* **12**, 82–86 (2015).
47. M. Zhao, *et al.*, Tumor-targeting bacterial therapy with amino acid auxotrophs of GFP-expressing Salmonella typhimurium. *Proc Natl Acad Sci U S A* **102**, 755–760 (2005).
48. C. Fan, *et al.*, Chromosome-free bacterial cells are safe and programmable platforms for synthetic biology. *Proc Natl Acad Sci U S A* **117**, 6752–6761 (2020).
49. B. Lim, *et al.*, Reprogramming Synthetic Cells for Targeted Cancer Therapy. *ACS Synth Biol* **11**, 1349–1360 (2022).
50. C. P. N. Rampley, *et al.*, Development of SimCells as a novel chassis for functional biosensors. *Scientific Reports 2017 7:1* **7**, 1–10 (2017).
51. S. L. Liu, A. Hessel, K. E. Sanderson, Genomic mapping with I-Ceu I, an intron-encoded endonuclease specific for genes for ribosomal RNA, in Salmonella spp., Escherichia coli, and other bacteria. *Proc Natl Acad Sci U S A* **90**, 6874 (1993).
52. C. Fan, *et al.*, Chromosome-free bacterial cells are safe and programmable platforms for synthetic biology. https://doi.org/10.25345/C5HD3F.
53. H. I. Adler, W. D. Fisher, A. Cohen, A. A. Hardigree, Miniature escherichia coli Cells Deficient in DNA. *Proceedings of the National Academy of Sciences* **57**, 321–326 (1967).
54. J. A. MacDiarmid, *et al.*, Bacterially Derived 400 nm Particles for Encapsulation and Cancer Cell Targeting of Chemotherapeutics. *Cancer Cell* **11**, 431–445 (2007).
55. J. Lutkenhaus, Assembly dynamics of the bacterial minCDE system and spatial regulation of the z ring. *Annu Rev Biochem* **76**, 539–562 (2007).
56. D. Thi Thanh Vinh, N. Tu Hoang Khue, Study on Minicell Generation of Lactobacillus acidophilus VTCC-B-871 for Drug Delivery ARTICLE INFO ABSTRACT. *J Appl Pharm Sci* **3**, 33–036 (2013).
57. DEPARTMENT OF HEALTH AND HUMAN SERVICES National Institutes of Health, NIH GUIDELINES FOR RESEARCH INVOLVING RECOMBINANT OR SYNTHETIC NUCLEIC ACID MOLECULES (NIH GUIDELINES). (2024).
58. EnGeneIC granted FDA "Fast-Track" Designation for Novel Armed Nanocell Drug Conjugate (ANDC) Pancreatic Cancer Therapeutic. (2023).
59. J. A. MacDiarmid, H. Brahmbhatt, Minicells: Versatile vectors for targeted drug or si/shRNA cancer therapy. *Curr Opin Biotechnol* **22**, 909–916 (2011).
60. S. M. Sagnella, *et al.*, Cyto-Immuno-Therapy for Cancer: A Pathway Elicited by Tumor-Targeted, Cytotoxic Drug-Packaged Bacterially Derived Nanocells. *Cancer Cell* **37**, 354-370.e7 (2020).
61. D. S. Glass, I. H. Riedel-Kruse, A Synthetic Bacterial Cell-Cell Adhesion Toolbox for Programming Multicellular Morphologies and Patterns. *Cell* **174**, 649-658.e16 (2018).
62. S. Pukatzki, *et al.*, Identification of a conserved bacterial protein secretion system in Vibrio cholerae using the Dictyostelium host model system. *Proc Natl Acad Sci U S A* **103**, 1528–1533 (2006).
63. J. D. Mougous, *et al.*, A virulence locus of Pseudomonas aeruginosa encodes a protein secretion apparatus. *Science (1979)* **312**, 1526–1530 (2006).
64. Y. Cui, *et al.*, Heterologous Assembly of the Type VI Secretion System Empowers Laboratory Escherichia coli with Antimicrobial and Cell Penetration Capabilities. *Appl Environ Microbiol* **88** (2022).
65. A. B. Russell, *et al.*, Type VI secretion delivers bacteriolytic effectors to target cells. *Nature* **475**, 343 (2011).
66. S. J. Coulthurst, The Type VI secretion system – a widespread and versatile cell targeting system. *Res Microbiol* **164**, 640–654 (2013).

67. L. P. Allsopp, P. Bernal, Killing in the name of: T6SS structure and effector diversity. *Microbiology (United Kingdom)* **169**, 001367 (2023).
68. I. Kocaçalıskocaçalıs¸kan, I. Talan, I. Terzi, "Antimicrobial Activity of Catechol and Pyrogallol as Allelochemicals" (2006).
69. N. Schweigert, A. J. B. Zehnder, R. I. L. Eggen, Chemical properties of catechols and their molecular modes of toxic action in cells, from microorganisms to mammals. *Environ Microbiol* **3**, 81–91 (2001).
70. S. Razaviamri, K. Wang, B. Liu, B. P. Lee, Catechol-Based Antimicrobial Polymers. *Molecules 2021, Vol. 26, Page 559* **26**, 559 (2021).
71. D. M. A. Costa, *et al.*, Catalytic mechanism for the conversion of salicylate into catechol by the flavin-dependent monooxygenase salicylate hydroxylase. *Int J Biol Macromol* **129**, 588–600 (2019).
72. S. Yamamotoj, M. Katagiri, H. Maeno, O. Hayaishi~, Salicylate Hydroxylase, a Monooxygenase* Requiring Flavin Adenine Dinucleotide I. PURIFICATION AND GENERAL PROPERTIES i. *Journal of Biological Chemistry* **240**, 3408–3413 (1965).
73. E. J. De Genst, *et al.*, Structure and properties of a complex of α-synuclein and a single-domain camelid antibody. *J Mol Biol* **402**, 326–343 (2010).
74. M. LeRoux, *et al.*, Quantitative single-cell characterization of bacterial interactions reveals type VI secretion is a double-edged sword. *Proc Natl Acad Sci U S A* **109**, 19804–19809 (2012).
75. T. Rollenske, *et al.*, Parallelism of intestinal secretory IgA shapes functional microbial fitness. *Nature 2021 598:7882* **598**, 657–661 (2021).
76. Y. G. Santin, T. Doan, L. Journet, E. Cascales, Cell Width Dictates Type VI Secretion Tail Length. *Current Biology* **29**, 3707-3713.e3 (2019).
77. B. J. Solomon, *et al.*, A First-Time-In-Human Phase I Clinical Trial of Bispecific Antibody-Targeted, Paclitaxel-Packaged Bacterial Minicells. *PLoS One* **10** (2015).
78. J. Yang, M. A. Cohen Stuart, M. Kamperman, Jack of all trades: Versatile catechol crosslinking mechanisms. *Chem Soc Rev* [Preprint] (2014).
79. D. E. Fullenkamp, D. G. Barrett, D. R. Miller, J. W. Kurutz, P. B. Messersmith, pH-dependent cross-linking of catechols through oxidation via Fe3+ and potential implications for mussel adhesion. *RSC Adv* **4**, 25127–25134 (2014).
80. H. Meng, Y. Li, M. Faust, S. Konst, B. P. Lee, Hydrogen peroxide generation and biocompatibility of hydrogel-bound mussel adhesive moiety. *Acta Biomater* **17**, 160–169 (2015).
81. H. Meng, *et al.*, Biomimetic recyclable microgels for on-demand generation of hydrogen peroxide and antipathogenic application. *Acta Biomater* **83** (2019).
82. J. X. Chen, *et al.*, Development of aspirininducible biosensors in Escherichia coli and SimCells. *Appl Environ Microbiol* **85** (2019).
83. M. KATAGIRI, S. YAMAMOTO, O. HAYAISHI, Flavin Adenine Dinucleotide Requirement for the Enzymic Hydroxylation and Decarboxylation of Salicylic Acid. *Journal of Biological Chemistry* **237**, PC2413–PC2414 (1962).
84. S. J. Kim, M. K. Oh, Minicell-forming Escherichia coli mutant with increased chemical production capacity and tolerance to toxic compounds. *Bioresour Technol* **371**, 128586 (2023).
85. S. J. Kim, W. Chang, M. K. Oh, Escherichia coli minicells with targeted enzymes as bioreactors for producing toxic compounds. *Metab Eng* **73**, 214–224 (2022).
86. H. L. Lee, *et al.*, Quantitative Proteomics Analysis Reveals the Min System of Escherichia coli Modulates Reversible Protein Association with the Inner Membrane. *Molecular & Cellular Proteomics* **15**, 1572–1583 (2016).
87. L. Wettmann, K. Kruse, The Min-protein oscillations in Escherichia coli: an example of self-organized cellular protein waves. *Philosophical Transactions of the Royal Society B: Biological Sciences* **373** (2018).

88. M. H. Nicolas-Chanoine, X. Bertrand, J. Y. Madec, Escherichia coli ST131, an Intriguing Clonal Group. *Clin Microbiol Rev* **27**, 543 (2014).
89. B. A. Rogers, H. E. Sidjabat, D. L. Paterson, Escherichia coli O25b-ST131: a pandemic, multiresistant, community-associated strain. *Journal of Antimicrobial Chemotherapy* **66**, 1–14 (2011).
90. M. H. Nicolas-Chanoine, *et al.*, Intercontinental emergence of Escherichia coli clone O25:H4-ST131 producing CTX-M-15. *Journal of Antimicrobial Chemotherapy* **61**, 273–281 (2008).
91. A. Colpan, *et al.*, Escherichia coli Sequence Type 131 (ST131) Subclone H30 as an Emergent Multidrug-Resistant Pathogen Among US Veterans. *Clinical Infectious Diseases* **57**, 1256–1265 (2013).
92. R. Banerjee, J. R. Johnson, A new clone sweeps clean: The enigmatic emergence of Escherichia coli sequence type 131. *Antimicrob Agents Chemother* **58**, 4997–5004 (2014).
93. World Health Organization, WHO Bacterial Priority Pathogens List, 2024- Bacterial pathogens of public health importance to guide research, development and strategies to prevent and control antimicrobial resistance. *World Health Organization* 1–72 (2024).
94. M. Sorgenfrei, *et al.*, Rapid detection and capture of clinical Escherichia coli strains mediated by OmpA-targeting nanobodies. *Commun Biol* **8**, 1–17 (2025).
95. B. J. Solomon, *et al.*, A First-Time-In-Human Phase I Clinical Trial of Bispecific Antibody-Targeted, Paclitaxel-Packaged Bacterial Minicells. *PLoS One* **10**, e0144559 (2015).
96. U. Mamat, *et al.*, Endotoxin-free protein production—ClearColi^{TM} technology. *Nature Methods 2013 10:9* **10**, 916–916 (2013).
97. D. L. Paterson, Antibacterial agents active against Gram Negative Bacilli in phase I, II, or III clinical trials. *Expert Opin Investig Drugs* **33**, 371–387 (2024).
98. G. Cheng, *et al.*, Antimicrobial Drugs in Fighting against Antimicrobial Resistance. *Front Microbiol* **7**, 470 (2016).
99. A. Focareta, J. C. Paton, R. Morona, J. Cook, A. W. Paton, A Recombinant Probiotic for Treatment and Prevention of Cholera. *Gastroenterology* **130**, 1688–1695 (2006).
100. F. Duan, J. C. March, Engineered bacterial communication prevents Vibrio cholerae virulence in an infant mouse model. *Proc Natl Acad Sci U S A* **107**, 11260–11264 (2010).
101. P. Jayaraman, M. B. Holowko, J. W. Yeoh, S. Lim, C. L. Poh, Repurposing a Two-Component System-Based Biosensor for the Killing of Vibrio cholerae. *ACS Synth Biol* **6**, 1403–1415 (2017).
102. I. Y. Hwang, *et al.*, Engineered probiotic Escherichia coli can eliminate and prevent Pseudomonas aeruginosa gut infection in animal models. *Nature Communications 2017 8:1* **8**, 1–11 (2017).
103. T. A. Hamilton, *et al.*, Efficient inter-species conjugative transfer of a CRISPR nuclease for targeted bacterial killing. *Nature Communications 2019 10:1* **10**, 1–9 (2019).
104. R. López-Igual, J. Bernal-Bayard, A. Rodríguez-Patón, J. M. Ghigo, D. Mazel, Engineered toxin–intein antimicrobials can selectively target and kill antibiotic-resistant bacteria in mixed populations. *Nature Biotechnology 2019 37:7* **37**, 755–760 (2019).
105. Y. G. Li, K. Kishida, N. Ogawa-Kishida, P. J. Christie, Ligand-displaying Escherichia coli cells and minicells for programmable delivery of toxic payloads via type IV secretion systems. *mBio* **14** (2023).
106. S. Muyldermans, Nanobodies: Natural single-domain antibodies. *Annu Rev Biochem* **82**, 775–797 (2013).
107. N. Y. Yu, *et al.*, Sequence analysis PSORTb 3.0: improved protein subcellular localization prediction with refined localization subcategories and predictive capabilities for all prokaryotes. **26**, 1608–1615 (2010).
108. C. McMahon, *et al.*, Yeast surface display platform for rapid discovery of conformationally selective nanobodies. *Nature Structural & Molecular Biology 2018 25:3* **25**, 289–296 (2018).

109. N. R. Bennett, *et al.*, Atomically accurate de novo design of single-domain antibodies. *bioRxiv* 2024.03.14.585103 (2024). https://doi.org/10.1101/2024.03.14.585103.
110. M. A. Rangel, *et al.*, Fragment-based computational design of antibodies targeting structured epitopes. *Sci Adv* **8**, 9540 (2022).
111. A. Ramon, *et al.*, Assessing antibody and nanobody nativeness for hit selection and humanization with AbNatiV. *Nature Machine Intelligence 2024 6:1* **6**, 74–91 (2024).
112. S. Y. Ting, *et al.*, Targeted Depletion of Bacteria from Mixed Populations by Programmable Adhesion with Antagonistic Competitor Cells. *Cell Host Microbe* **28**, 313-321.e6 (2020).
113. B. Jana, K. Keppel, D. Salomon, Engineering a customizable antibacterial T6SS-based platform in Vibrio natriegens. *EMBO Rep* **22**, e53681 (2021).
114. N. H. Le, V. Pinedo, J. Lopez, F. Cava, M. F. Feldman, Killing of Gram-negative and Gram-positive bacteria by a bifunctional cell wall-targeting T6SS effector. *Proc Natl Acad Sci U S A* **118**, e2106555118 (2021).
115. J. Kreitz, *et al.*, Programmable protein delivery with a bacterial contractile injection system. *Nature 2023 616:7956* **616**, 357–364 (2023).
116. S. J. Hersch, L. Lam, T. G. Dong, Engineered Type Six Secretion Systems Deliver Active Exogenous Effectors and Cre Recombinase. *mBio* **12** (2021).
117. S. Coulthurst, The Type VI secretion system: A versatile bacterial weapon. *Microbiology (United Kingdom)* **165**, 503–515 (2019).
118. M. J. Giacalone, *et al.*, The use of bacterial minicells to transfer plasmid DNA to eukaryotic cells. *Cell Microbiol* **8**, 1624–1633 (2006).
119. M. Jivrajani, N. Shrivastava, M. Nivsarkar, A combination approach for rapid and high yielding purification of bacterial minicells. *J Microbiol Methods* **92**, 340–343 (2013).

909 **Main Figures**

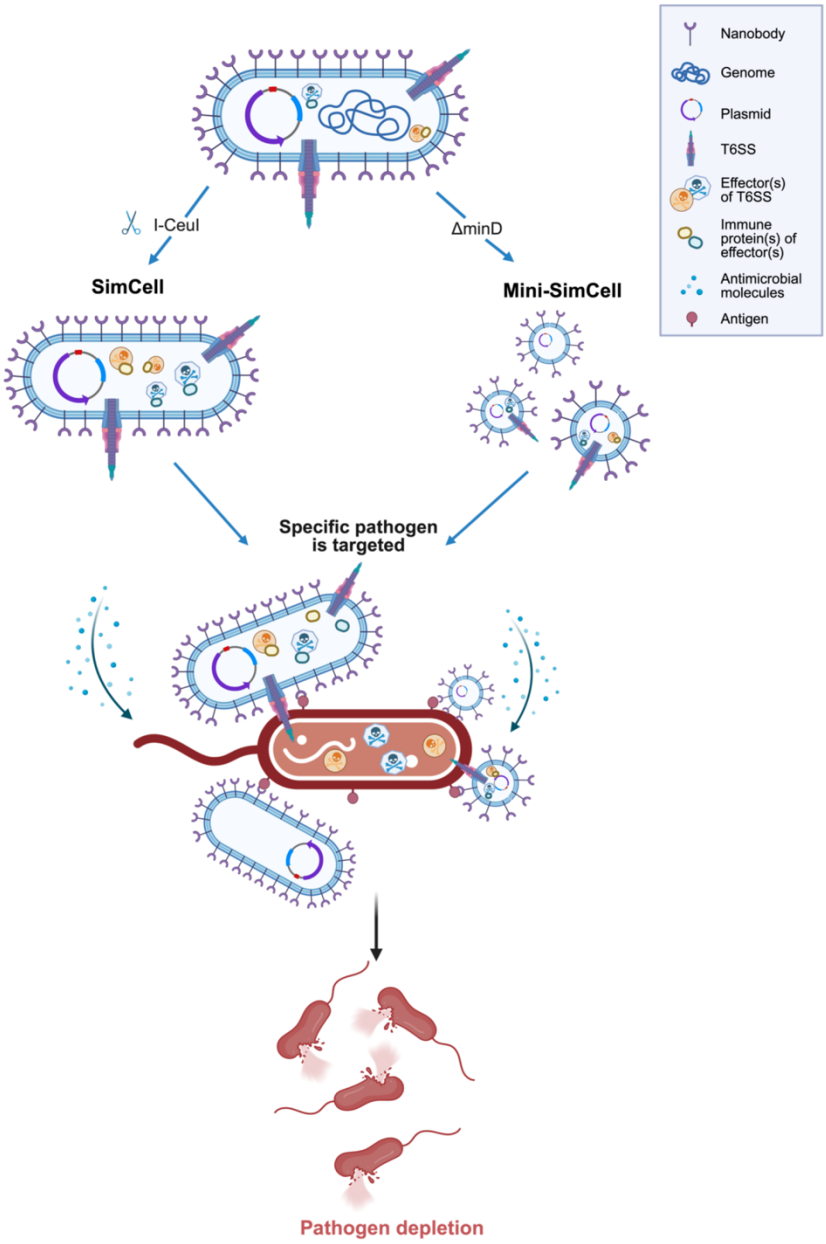

910

911 **Figure 1. Design of the SimCell and mini-SimCell platform for treating bacterial AMR.** Surface-
912 displayed nanobodies are engineered to the outer membrane of SimCell and mini-SimCell using a
913 modular surface display system, to enable antigen recognition and selectively binding to target
914 pathogens. This nanobody-antigen binding is expected to increase the specificity, shorten the distance,
915 and enhance the efficiency of contact-dependent or enhanced inhibition mechanisms including toxic
916 effector protein delivery through modularised T6SS and localised antimicrobial molecules generation.

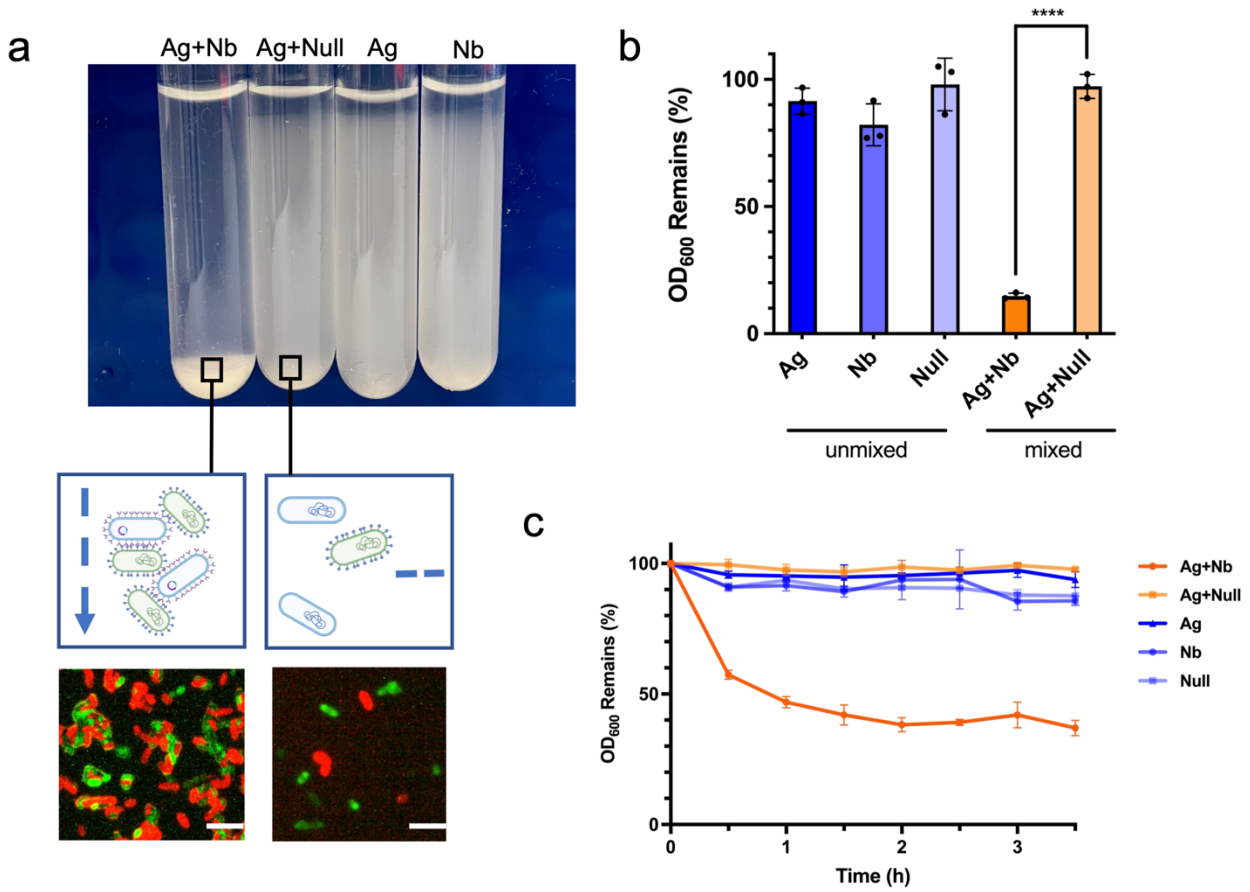

Figure 2. Surface-displayed nanobody in engineered *E. coli* enables selective cell-cell binding via nanobody-antigen interactions. **(a)** Binding of Ag and Nb cells in a 1:1 ratio leads to both detectable macroscopic and microscopic aggregation compared to unmixed and non-adhesion (Ag+Null) conditions. Red: mRFP-labelled Nb/Null cells. Green: sfGFP-labelled Ag cells. Scale bar, 10 µm. **(b)** Ag-Nb aggregating cell mixture shows significant settling compared to unmixed and non-adhesion (Ag-Null) conditions after 12 hrs. **(c)** Time courses of macroscopic aggregation show significant settling within ~ 30 min. All cell cultures were mixed at time 0 and allowed to settle. OD_{600} from top 25% supernatant was continuously measured every 30 min for 3.5 hrs. For **(b)** and **(c)**, all cultures were normalised to the same initial OD_{600} and mixed in 1:1 v/v ratio. N = 3 replicates, Error bars, ±1 SD, ****$p < 0.0001$ according to a 2-tailed paired t-test.

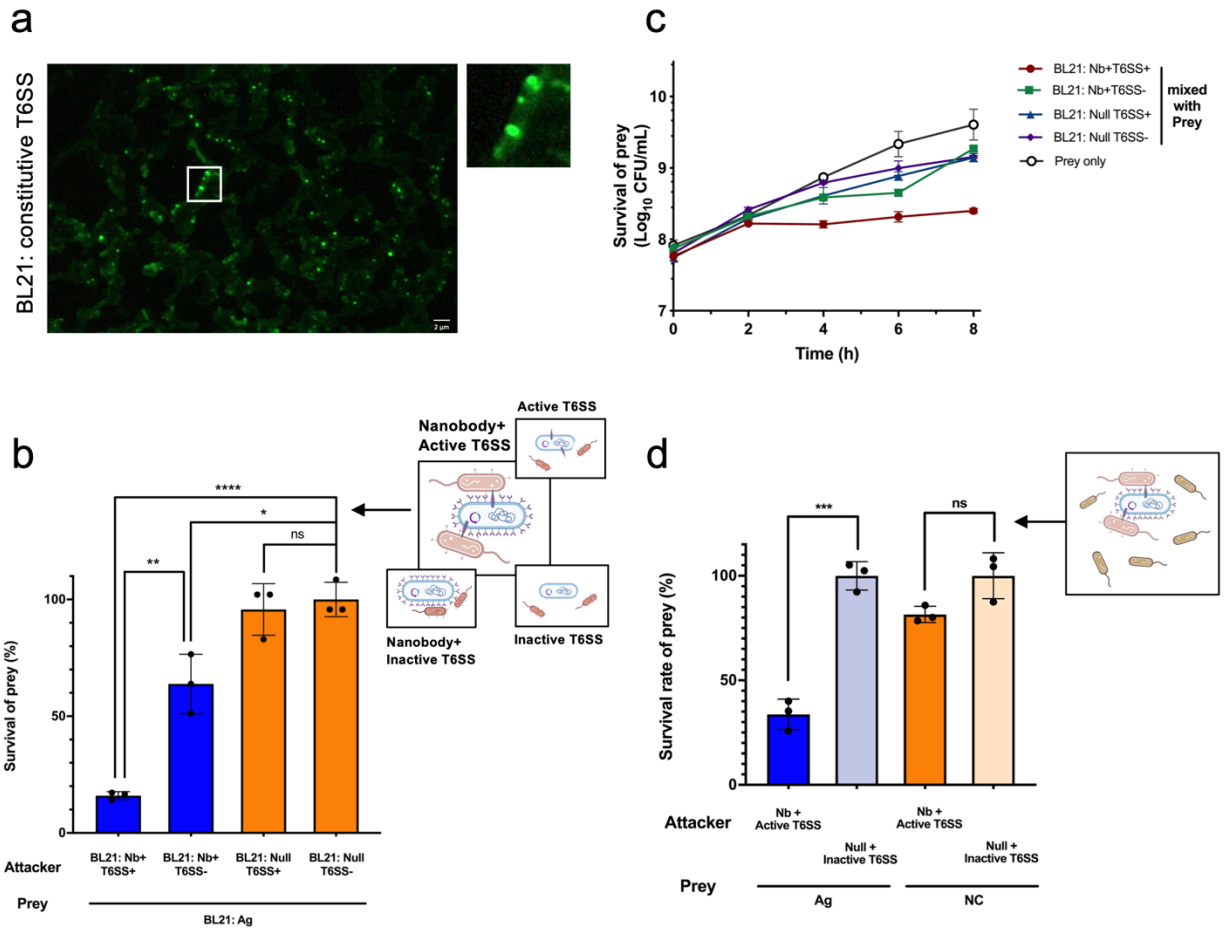

Figure 3. Nanobody-antigen mediated cell-cell adhesion enables selectively depletion of target cells via T6SS in liquid condition. (a) Fluorescence microscopic analysis confirms the assembly of T6SS in laboratory *E. coli* strain BL21(DE3). C-terminal sfGFP was fused to VipA for labelling. Localised fluorescence signals were observed. Scale bar, 2 µm. **(b)** Nanobody-antigen binding enables an efficient T6SS-mediated killing in liquid condition. Incubation time = 6h. Attacker : prey v/v ratio = 10:1. In the schematic, target cells with surface antigen and programmed attacker cells (Nb+T6SS+ / Nb+T6SS- / Null T6SS+ / Null T6SS-) are represented. Nb+ = cells with surface-displayed nanobody, Null = cells with no adhesin. T6SS+ = cells with active induced T6SS, T6SS- = cells with inactive induced T6SS. **(c)** Time courses of nanobody-enhanced T6SS killing effect in liquid condition. Significant killing was observed after 2 hours. Incubation time =0, 2, 4, 6, 8 hr. Attacker : prey v/v ratio = 10:1. **(d)** Nb-Ag recognition enables a specific T6SS-mediated killing in liquid condition. In the schematic, programmed attacker cells (Nb+T6SS+) and Prey 1 (Ag), Ag-expressed *E. coli* BL21, prey 2 (NC), *E. coli* DH10B are represented. Incubation time = 6 hr. Attacker : prey 1: prey 2 v/v ratio = 10:1:1. For **(b)** to **(d)**, all cultures were normalised to the same initial OD_{600}. N = 3 replicates, Error bars, ±1 SD, *p < 0.1, **p < 0.01, ***p < 0.001, ****p < 0.0001 according to a 2-tailed paired t-test. Survival rate was calculated as survival cells/ total prey cells.

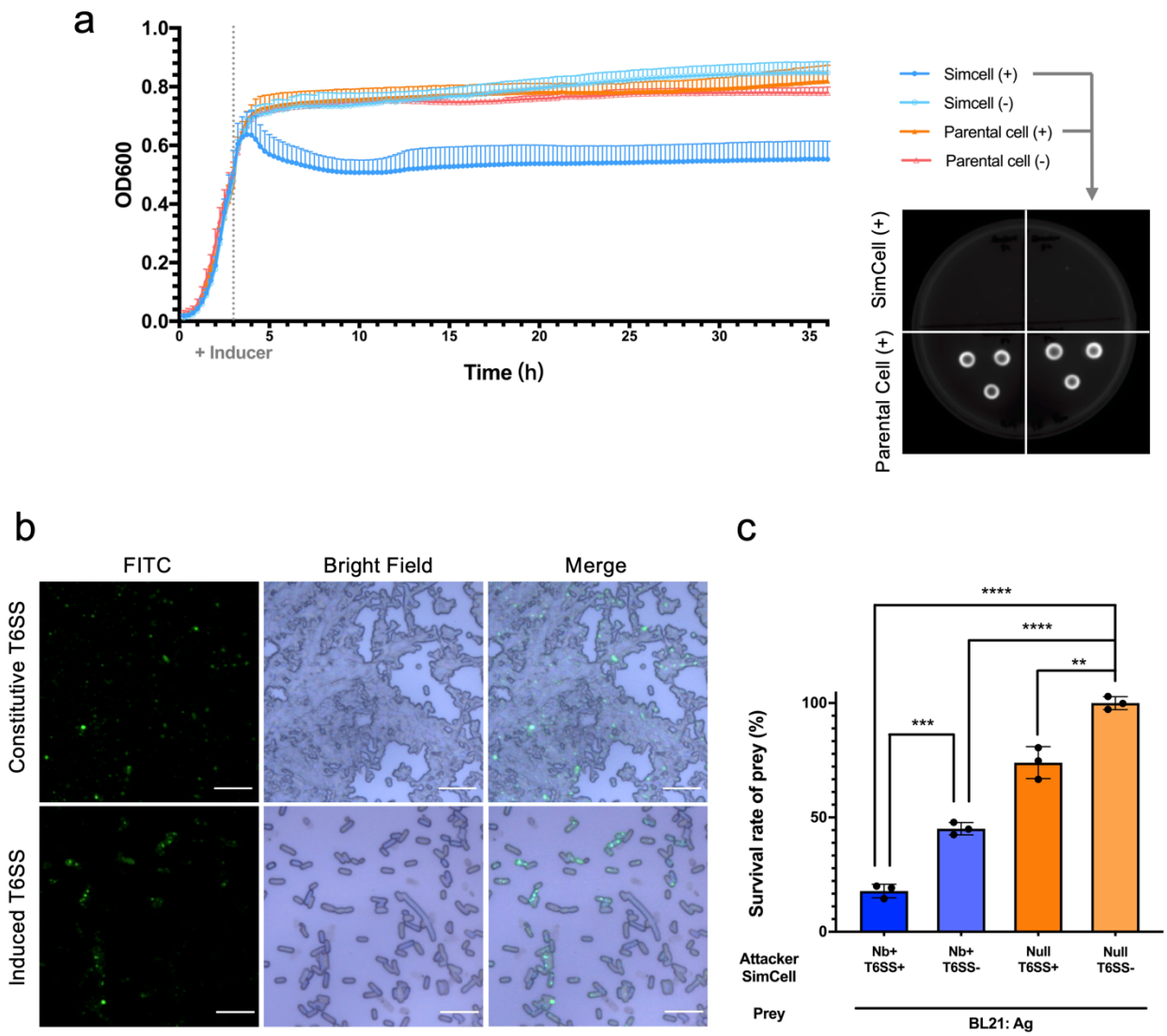

Figure 4. T6SS-mediated killing in reprogrammed SimCells. (a) SimCell conversion and purity check. Growth assays confirm the successful SimCell conversion from the engineered parent cell. OD_{600} was continuously measured every 15 min to monitor the growth curve over 35 hours. The grey dot vertical line indicates the time point (3h after initial incubation) of inducer addition (1 μM crystal violet). Growth arrest was observed shortly after inducer addition for induced SimCells. n = 3 replicates, Error bars, ±1 SD. Agar plate culturing confirmed a high efficiency of SimCell conversion. All cultures were plated on LB agar plates and incubated for 24 hours at 37 °C. **(b)** Fluorescence microscopic analysis confirms the assembly of T6SS in *E. coli* strain BL21(DE3)-derived SimCells. Scale bar, 10 μm. **(c)** Nanobody-antigen binding enhances T6SS-mediated killing in SimCells in liquid condition. Incubation time = 6 hr. Attacker : prey v/v ratio = 10:1. N = 3 replicates, Error bars, ±1 SD, $^{**}p < 0.01$, $^{***}p < 0.001$, $^{****}p < 0.0001$ according to a 2-tailed paired t-test. Survival rate was calculated as survival cells/ total prey cells.

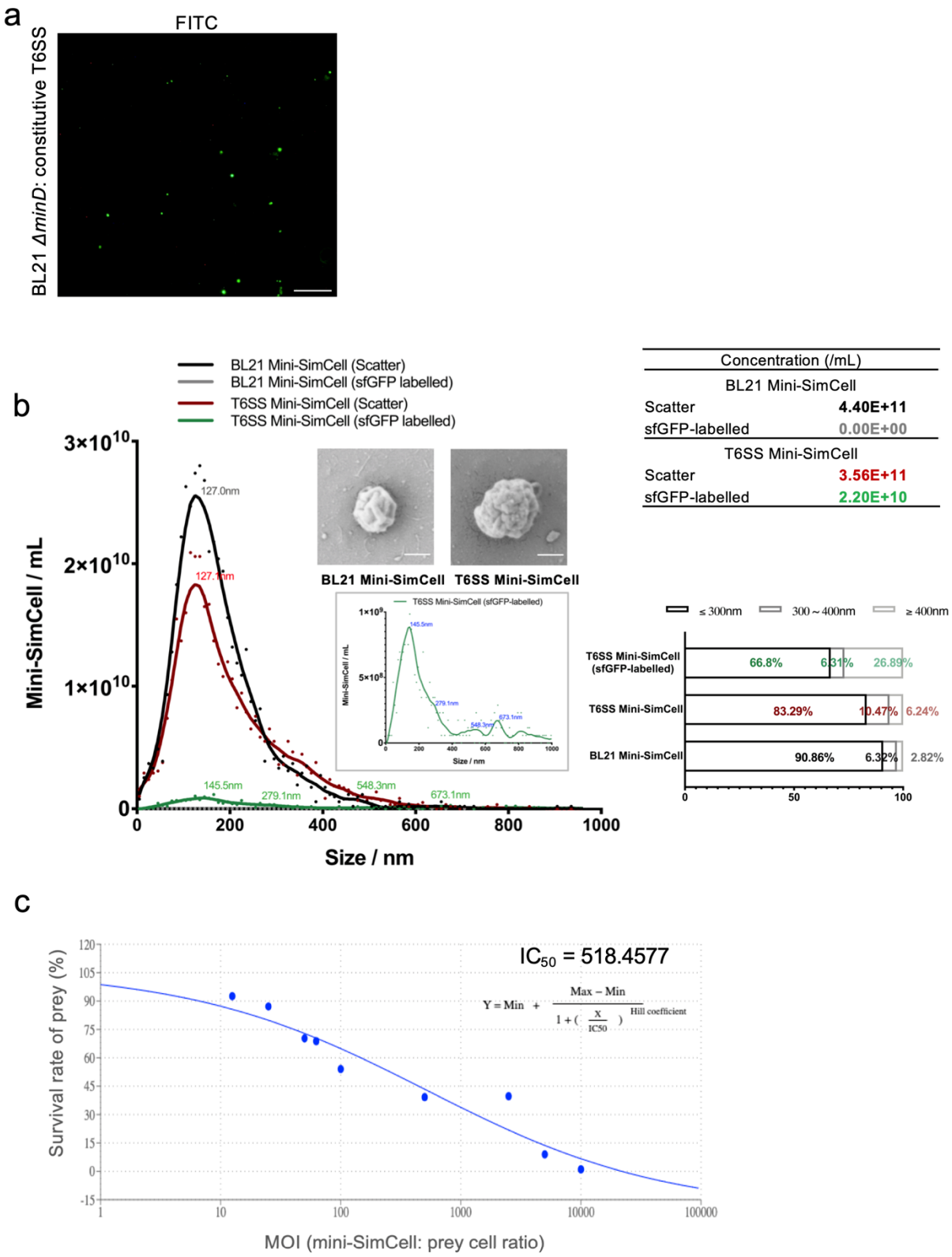
a
FITC
BL21 ΔminD: constitutive T6SS
b
BL21 Mini-SimCell (Scatter)
BL21 Mini-SimCell (sfGFP labelled)
T6SS Mini-SimCell (Scatter)
T6SS Mini-SimCell (sfGFP labelled)
Mini-SimCell / mL
Size / nm
127.0nm
145.5nm
279.1nm
548.3nm
673.1nm
BL21 Mini-SimCell
T6SS Mini-SimCell
Concentration (/mL)
BL21 Mini-SimCell
Scatter 4.40E+11
sfGFP-labelled 0.00E+00
T6SS Mini-SimCell
Scatter 3.56E+11
sfGFP-labelled 2.20E+10
≤ 300nm
300 ~ 400nm
≥ 400nm
T6SS Mini-SimCell (sfGFP-labelled) 66.8% 6.31% 26.89%
T6SS Mini-SimCell 83.29% 10.47% 6.24%
BL21 Mini-SimCell 90.86% 6.32% 2.82%
c
IC50 = 518.4577
Survival rate of prey (%)
MOI (mini-SimCell: prey cell ratio)

959

960

961 **Figure 5. T6SS-mediated killing in mini-SimCells. (a)** Fluorescence microscopic analysis confirms
962 the assembly of T6SS in *E. coli* BL21(DE3)-derived mini-SimCells. Scale bar, 10 μm. **(b)** Size
963 distribution characterisation of mini-SimCells derived from BL21 parental cells with/without T6SS
964 (T6SS/BL21 mini-SimCells). ZetaView was used for the characterisation of mini-SimCell size
965 distribution and concentration. Scanning electron microscope images of mini-SimCells derived from
966 BL21 parental cells with/without T6SS (T6SS/BL21 mini-SimCells). Magnification, 50,000X. Scale
967 bar, 200nm. **(c)** The inhibitory concentration curve of T6SS-assembled mini-SimCells in liquid
968 condition. A half-maximal inhibitory concentration (IC_{50}) is around 518.5 T6SS-mini-SimCells per
969 prey cell. N = 3 replicates. Survival rate was calculated as survival cells/ total prey cells.

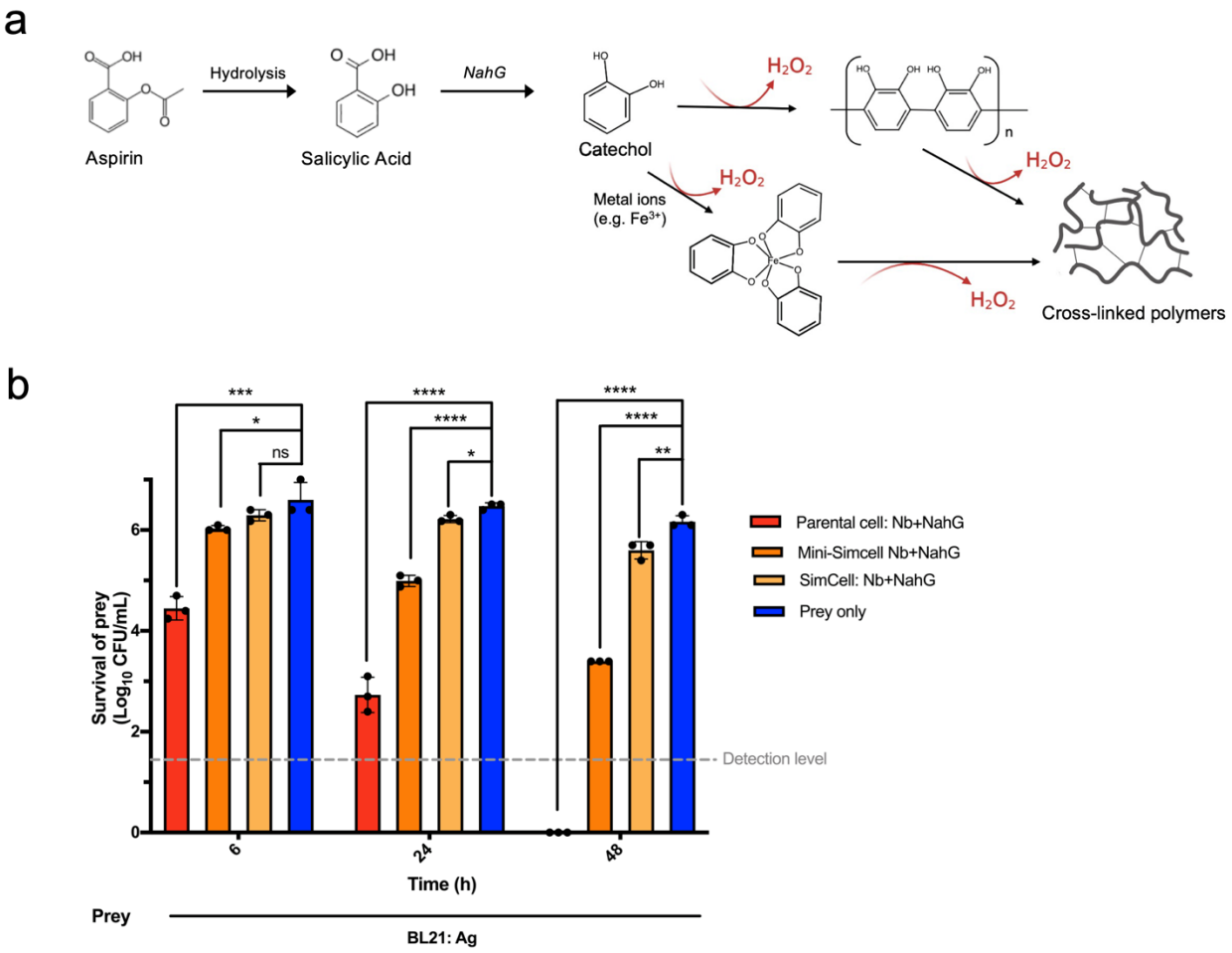

Figure 6. Reprogrammed parental cells and (mini-) SimCells enables localised generation of antimicrobial compound – catechol. (a) Schematic illustration of aspirin hydrolysis to salicylic acid, followed by the generation of catechol catalysed by the NahG enzyme. The auto-oxidation of catechol and cross-linking results in the release of H_2O_2. **(b)** Inhibitory efficiency of localised catechol-producing parental cells / SimCells / Mini-SimCells in liquid condition. Attacker : prey n:n ratio = Parental cells / SimCells / Mini-SimCells 10/100:1,000:1. N = 3 replicates, Error bars, ±1 SD, *$p < 0.1$, **$p < 0.01$, ***$p < 0.001$, ****$p < 0.0001$ according to a 2-tailed paired t-test.

a

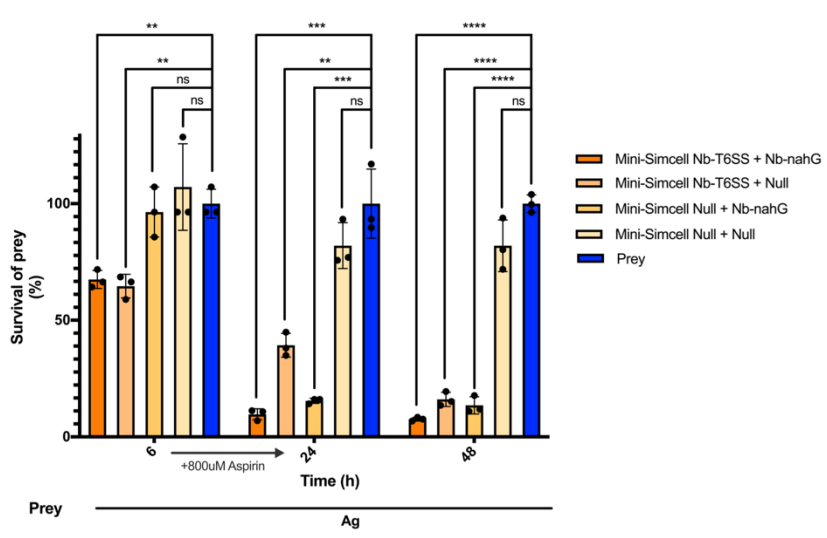
Survival of prey (%)
Time (h)
+800uM Aspirin
Prey
Ag
Mini-Simcell Nb-T6SS + Nb-nahG
Mini-Simcell Nb-T6SS + Null
Mini-Simcell Null + Nb-nahG
Mini-Simcell Null + Null
Prey

b

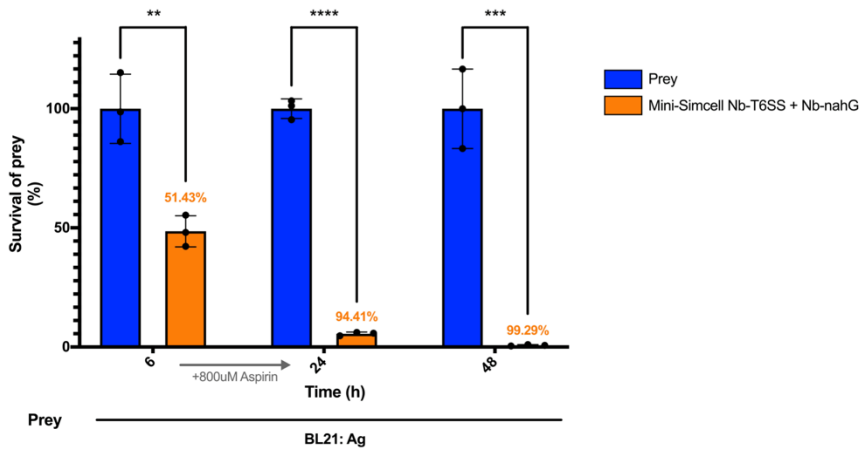
Survival of prey (%)
51.43%
94.41%
99.29%
Time (h)
+800uM Aspirin
Prey
BL21: Ag
Prey
Mini-Simcell Nb-T6SS + Nb-nahG

c

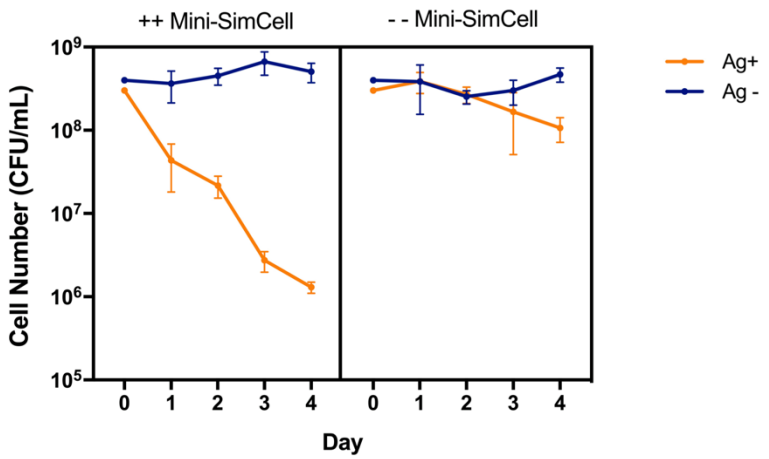
++ Mini-SimCell
- - Mini-SimCell
Cell Number (CFU/mL)
Day
Ag+
Ag -

978

Figure 7. Selective elimination efficiency of the consortium with dual-mechanism mini-SimCells in liquid condition. (a) Two different attackers (Attaker1: mini-SimCell Nb-T6SS; Attaker2: mini-SimCell Nb-nahG) were mixed with prey cells in n:n ratio of Attacker1: Attacker2 : prey = 250:250:1, total Attacker cells were 5×10^{9}, within the maximum tolerated dose (MTD) reported in the previous human trial. All cultures were incubated at 37 °C and sampled from 6, 24, 48 hr. Aspirin of 800 μM was added after 6 hr. **(b)** Dual-mechanism mini-SimCell inhibition efficiency in MTD for humans. Two different attackers (Attaker1: mini-SimCell Nb-T6SS; Attaker2: mini-SimCell Nb-nahG) were mixed with prey cells in n:n ratio of Attacker1 : Attacker2 : prey = 500:500:1, total Attacker cells were 1×10^{10}, the MTD reported in the previous human trial. All cultures were incubated at 37 °C and sampled from 6, 24, 48 hr. Aspirin of 800 μM was added after 6 hr. **(c)** Selective elimination of targeted bacteria population in mixed communities using multi-dose dual-mechanism mini-SimCell consortium. Mixed prey cell populations with or without recognisable antigens (Ag+ or Ag-) were inoculated in n:n ratio of 1:1 for continuous co-culture at 37 °C. 1/50 dilution with fresh medium was conducted every 24 hrs, followed by 8 hrs of recovery growth, then introduction of a dose of mini-SimCell consortium and 16 hrs of co-incubation. For every dose of engineered mini-SimCell (++ Mini-SimCell), two different attackers (Attaker1: mini-SimCell Nb-T6SS; Attaker2: mini-SimCell Nb-nahG) were mixed in n:n ratio of 1:1, total attacker were 1×10^{12} mini-SimCells. For - - Mini-SimCell group, 1×10^{12} of non-engineered mini-SimCell were used. All cultures were incubated at 37 °C and sampled every 24 hrs. Aspirin of 800 μM was added with fresh medium. For **(a)** to **(c)**, N = 3 replicates, Error bars, ±1 SD, **$p < 0.01$, ***$p < 0.001$, ****$p < 0.0001$ according to a 2-tailed paired t-test. Survival rate was calculated as survival cells/ total prey cells. Killing efficiency = 1-survival rate.

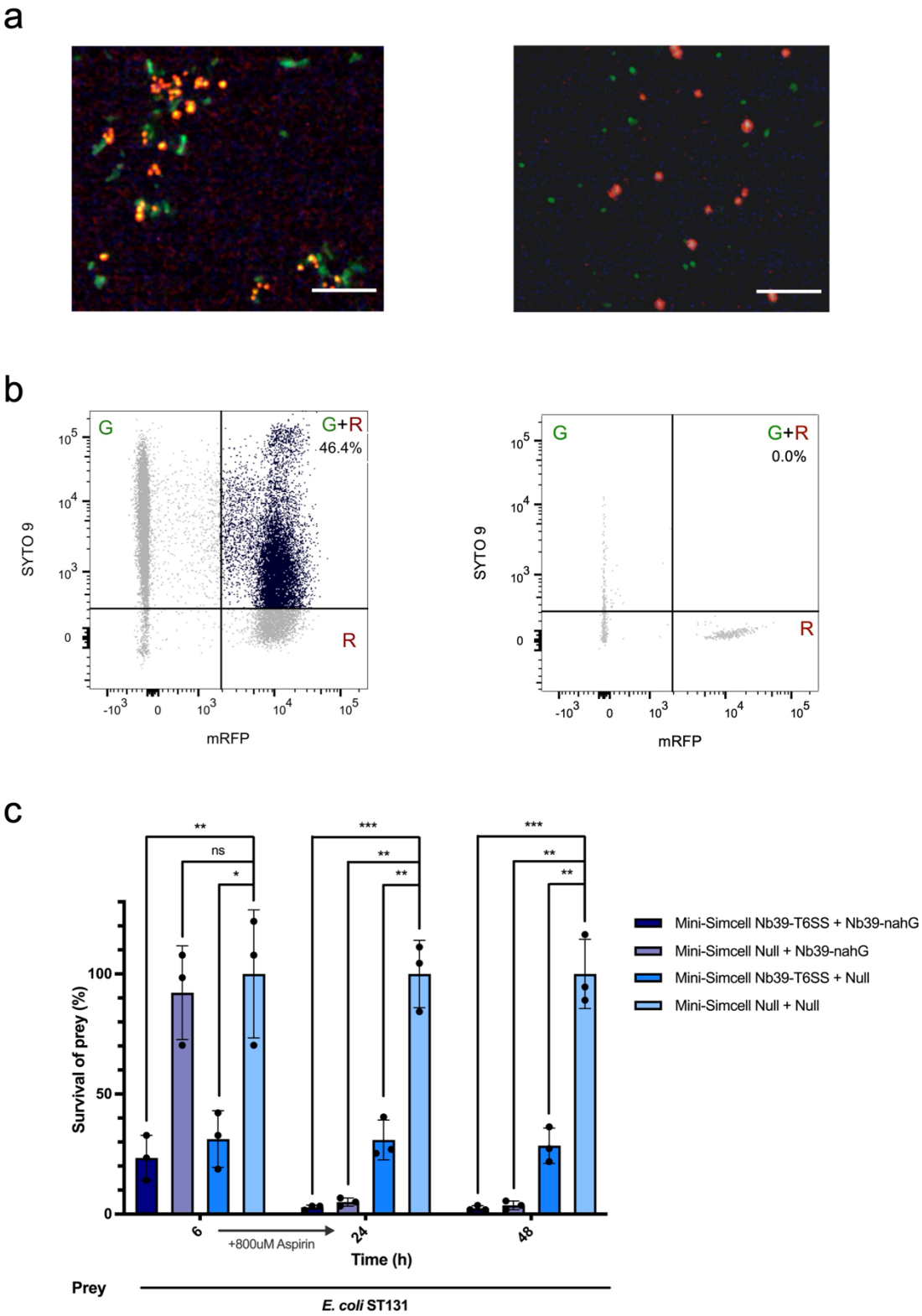

Figure 8. Reprogrammed mini-SimCells to kill a resistant pathogenic *E. coli* strain (*E. coli* ST131) by targeting a native antigen (OmpA-L). (a) Binding assay: *E. coli* ST131 and mini-SimCell parental strain BL21: Nb39_mRFP were mixed 1:1 ratio, leading to significant aggregation due to the

1005 Nb39-OmpA-L interaction, under fluorescence microscope (left). BL21: Ag and BL21: Nb39_mRFP
1006 cells were mixed with as unbinding negative control (right). Red: BL21: Nb39_mRFP cells. Green:
1007 SYTO 9 stained *E. coli* ST131 cells (left), SYTO 9 stained BL21: Ag cells (right). Scale bar, 10 μm.
1008 **(b)** Flow cytometry assay: Quantification of Nb39-mediated *E. coli* ST131 binding using a double-
1009 color events. Events of doublets formation (G+R) indicates the binding of *E. coli* ST131 and BL21:
1010 Nb39_mRFP. BL21: Ag and BL21: Nb39_mRFP mixture was the unbinding negative control. *E. coli*
1011 ST131 (left)/BL21: Ag (right) : BL21: Nb39_mRFP cell = 1:1. **(c)** Inhibitory efficiency of the
1012 consortium with dual-mechanism mini-SimCells against *E. coli* ST131. Two different attackers
1013 (Attaker1: mini-SimCell Nb39-T6SS; Attaker2: mini-SimCell Nb39-nahG) were mixed with prey cells
1014 in n/n ratio of Attacker1: Attacker2: prey = 500:500:1, showing elimination effect over 70%, 97% and
1015 97% at 6, 24 and 48 hrs. All cultures were incubated at 37 °C and sampled from 6, 24, 48 hrs. Aspirin
1016 of 800 μM was added after 6h. N = 3 replicates, Error bars, ±1 SD, *$p < 0.1$, **$p < 0.01$, ***$p < 0.001$
1017 according to a 2-tailed paired t-test. Survival rate was calculated as survival cells/ total prey cells;
1018 killing efficiency = 1-survival rate.